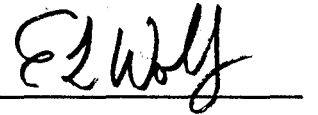**USING BALLISTIC ELECTRON EMISSION MICROSCOPY**

TO INVESTIGATE THE METAL-VACUUM INTERFACE

DISSERTATION

Submitted in Partial Fulfillment

of the Requirements for the

Degree of

DOCTOR OF PHILOSOPHY (Physics)

at the

POLYTECHNIC UNIVERSITY

by

Mevlana Celalettin Baykul

June 1993

Approved:

E L Wolf
_____

Department Head

Copy No._____

June 20 19 93

Approved by the Guidance Committee:

Major: Physics

_____

Sarath C. Meepagala

Assistant Professor of Physics

Minor: Material Science

_____

Said Nourbakhsh

Associate Professor of

Material Science

_____

Edward L. Wolf

Professor of Physics

_____

Carol Thompson

Assistant Professor of Physics

Microfilm or other copies of this
dissertation are obtainable from:

Dedicated to

my parents

ACKNOWLEDGMENTS

AN ABSTRACT

USING BALLISTIC ELECTRON EMISSION MICROSCOPY TO
INVESTIGATE THE METAL-VACUUM INTERFACE

by

Mevlana Celalettin Baykul

Advisor:Sarath C. Meepagala.

Submitted in Partial Fulfillment of the

Requirements for the Degree of

Doctor of Philosophy (Physics)

June 1993

This dissertation investigates the possibility of using the ballistic electron microscope (BEEM) to study the metal-vacuum interface. In order to do that, we have designed and built a novel experimental set-up which consists of an STM tip from which electrons tunnel into a thin (< 60 nm), free-standing metal film in vacuum ambient. When the tunnel bias exceeds the work function of the metal, some small fraction of the tunneling electrons traverses through the film without any energy loss, and emits into the vacuum through the back side

of the film. The rate of emission of such ballistic electrons, which is called the collector current, is measured by a channel electron multiplier.

One of the major challenges for this investigation was preparing free-standing thin films. We found that we can prepare good-quality free-standing Au thin films by the following steps: a) evaporating Au onto a (100) face of NaCl at room temperature, b) dissolving the NaCl in a 50-50 mixture of ethyl alcohol and distilled water, and c) catching the Au film that floats on the surface of the solvent onto a Cu grid. Subsequent annealing increased the grain size, and improved the bonding of the film onto the grid.

We have succeeded in observing ballistic electron emission through these free-standing thin films, even though the collector current tended to decay in a time interval of a few tenths of a second. The exact cause of this decay is not known, however we have suggested some possibilities. By ramping the bias voltage from about 0.2 V to about 10.5 V, we find the threshold bias voltage at which the collector current begins. This threshold voltage is an upper limit for the work function of Au. From our data we obtained a value of 5.2 V for this upper limit. We also have plotted the collector current, that was averaged over an scan area of 375 nm x 375 nm, against the tunnel bias. This plot shows that, for this region, the lowest threshold bias voltage for ballistic electron emission is between 3.5 V and 4.5 V.

We have obtained also a collector-current image that showed spatial variations of the collector current.

TABLE OF CONTENTS

TABLES OF FIGURES

CHAPTER I

INTRODUCTION

I.1   Scanning Tunneling Microscope

In 1981, Gerd Binnig and Heinrich Rohrer invented the scanning tunneling microscope (STM).[1] The STM consists of two electrodes, the tip and the sample. A schematic diagram of the STM is shown in Fig. 1. The tip is mounted on a piezoelectric translator that moves it in the XYZ directions with sub-nanometer resolution. Here, the plane of the sample is the XY plane, and the direction normal to the sample is the Z direction. Piezoelectric translators achieve these motions by changing their physical dimensions. These changes are induced by applying voltages to the electrodes that are placed on the piezoelectric elements. The tip approaches the sample through some form of coarse- and fine-positioning mechanism, until the tip-sample spacing is a few tenths of a nanometer. When a small bias voltage, such as 0.1 V, is applied to the tip, a small current (of the order of a few nA) can be established between the tip and the sample. This current is due to the electrons tunneling through the vacuum. In a typical operation of the
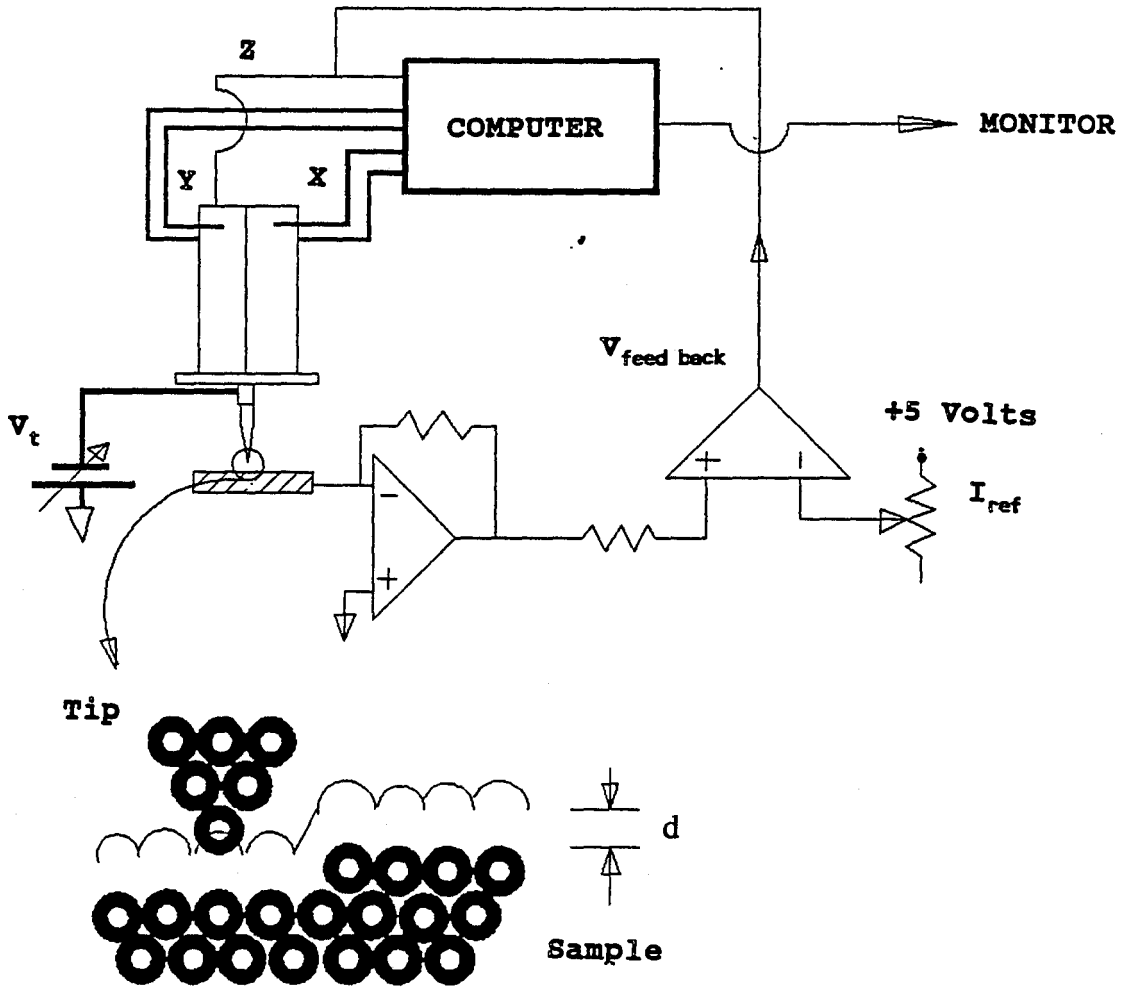
FIG. 1. Schematic diagram of the STM.

STM, the tunnel current is kept constant by a feedback mechanism which maintains the appropriate height of the tip above the sample, through the application of the required voltage to the piezoelectric translator in the Z direction (the Z-piezo). The tunnel current varies exponentially with the distance between the tip and the sample as follows,[2]

$$I \propto (\frac{V}{d}) \; e^{-A \, \phi^{1/2} \, d} \tag{1}$$

where V is the voltage between the tip and the sample, d is the distance between the tip and the sample, ϕ is the average work function of the tip and the sample in the units of eV , and A = 10.25 (eV)$^{-1/2}$ nm^{-1}. Thus the surface topography of a sample can be obtained by mapping the voltage that is applied to the Z-piezo, while the tip is raster-scanned over the sample, with the tunnel current kept constant. As the tunnel current is concentrated in an area of atomic dimensions, the STM is capable of yielding surface topography with atomic resolution. This high resolution surface imaging capability of an STM has helped many investigators in tackling many different problems. One of the famous problems that the use of the STM has settled is the imaging of the structure of a 7x7 reconstructed silicon surface.[3,4]

Besides imaging surface topography, the STM is also capable of producing electronic information on a sample through tunneling spectroscopy. This is done by studying the dependence of the tunnel current on the bias voltage. The local

density of states can be obtained from a plot of dI/dV versus V since,

$$\frac{dI}{dV} \propto \rho(r, V) \, D(V) \qquad (2)$$

where $\rho(r,V)$ is the local density of states of the sample, and D(V) is the transmission coefficient.[2,5] This type of measurement has yielded information on the band structures of semiconductors,[6] the energy gaps of superconductors,[7,8] and the coulomb blockade effects on small structures.[9] Also studied is the so-called "atom-resolved chemistry," which means the difference in I-V curves due to individual ad-atoms or molecules on sample surfaces.[10]

Apart from the above examples, the STM has been instrumental in novel studies in many diverse areas. For example, STM's have been operated in electrochemical cells for the purpose of investigating electrochemical reactions.[11,12] STM's have been used in biological studies such as imaging DNA, viruses, etc.[13,14] Also, STM's are being used in nano-lithography and pattern formation.[15] In recognition of the merits of the STM, its inventors, Binnig and Rohrer, were honored with the 1986 Nobel Prize in Physics.

I.2   Ballistic Electron Emission Microscope

Although the STM is a versatile tool for studies requiring high spatial resolution, the STM can see only the surface of a conducting sample. There are many instances where one would like to study sub-surface structures or the properties of a buried interface. For example, in device technology, it is very important to know the electronic and structural properties of the interfaces between metals and semiconductors. In order to address this particular problem, Kaiser and Bell developed, in 1988, a new experimental set-up that is based on the STM. They called their device the Ballistic Electron Emission Microscope (BEEM).[16] The BEEM consists of three electrodes: the tip, the base, and the collector (sketched in Fig. 2a). The tip of the BEEM acts just like the tip of the STM. The base component of the BEEM corresponds to the sample in the STM set-up. However, unlike an STM sample, the base is a very thin (about 10 nm) metal film, usually gold, that is deposited on an appropriate n-type semiconductor. This n-type semiconductor is called the collector (which is the third electrode in the BEEM). The tip is biased such that electrons tunnel from the tip to the base. Separate electrical leads are attached to the base and to the collector. A large fraction of the electrons that tunnel into the base gets scattered in the base, and finally conducts out through the base electrical lead. However, some electrons traverse through the base unscattered and impinge on the

Tip   Base   Collector

(a)

(b)

Tip   Base   Collector
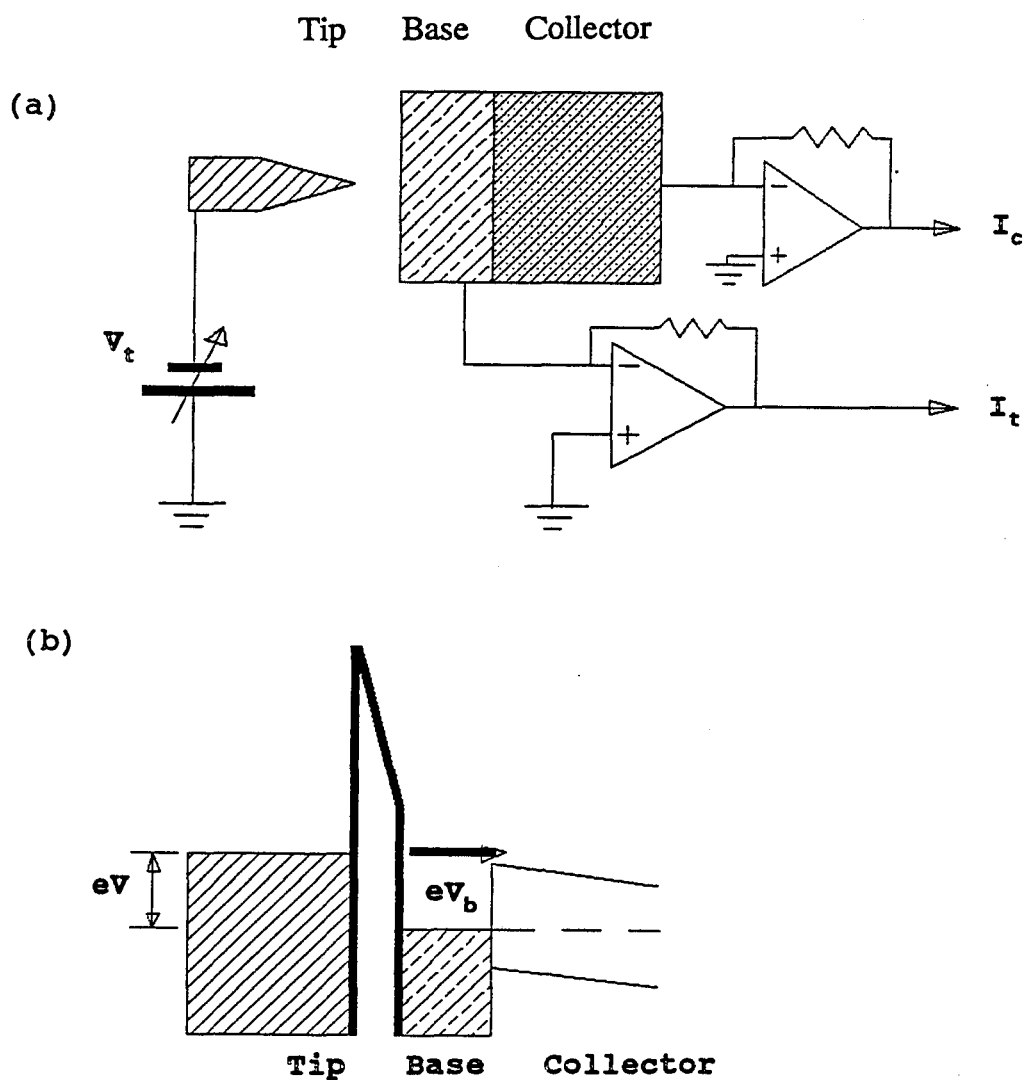
FIG. 2. (a) Schematic diagram of the BEEM set-up, (b) Energy diagram for BEEM of a metal-semiconductor schottky barrier system. Applied bias voltage between the tip and the base, in excess of the interface barrier V_b.

metal-semiconductor interface. If these electrons have sufficient energy to surmount the Schottky barrier at the interface, some fraction of them will enter the semiconductor, giving rise to a current through the collector lead. This current is called the collector current and is monitored by an electrometer.

The Schottky barrier, which is a potential barrier for the electrons, is formed at the metal-semiconductor interface, provided that the Fermi level of the metal is lower than that of the semiconductor.[17,18] This is the case for the Au-Si interface. In this situation, when the metal is brought to contact with the semiconductor, electrons transfer from gold to silicon, until the Fermi levels become equal. This transfer causes the metal surface to be negatively charged and the region of the semiconductor that is next to the metal surface, that is the depletion region, to have excess positive charge. The end result of this is the bending of the bands of the semiconductor towards higher energies in the vicinity of the interface. An electron entering the semiconductor from the metal will see a potential barrier of maximum height that is equal to $\phi_m - \phi_c$, where ϕ_m is the work function of the metal, and ϕ_c is the energy difference between the bottom of the conduction band of the semiconductor and the vacuum level. Fig. 3. shows an energy level diagram for the metal and the semiconductor before and after contact.

By mapping the collector current at a fixed bias voltage,

METAL   SEMICONDUCTOR
n-type

(a)

(b)
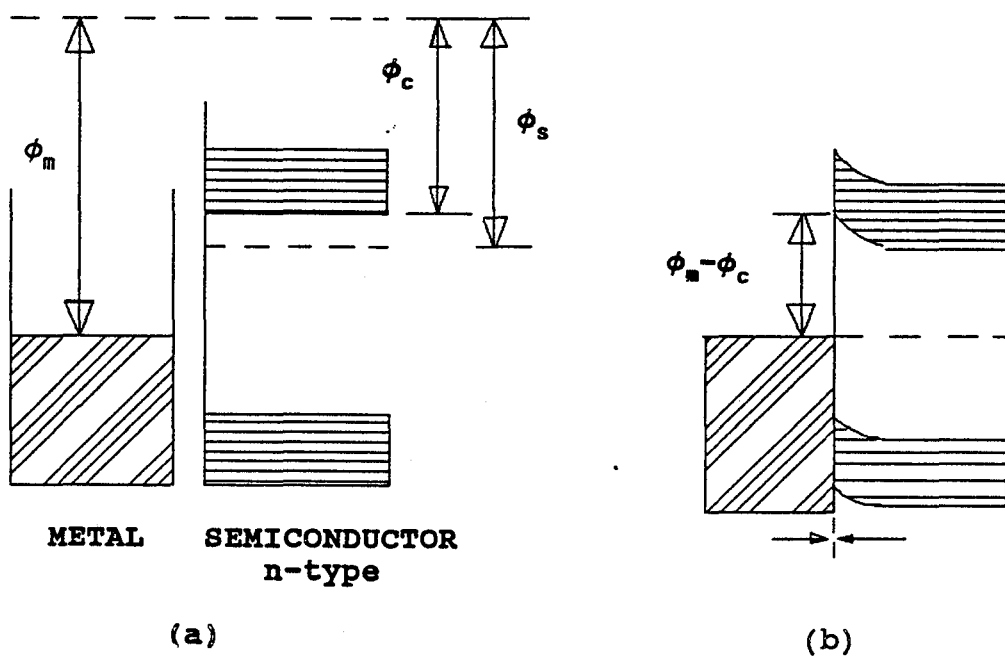
FIG. 3. Energy band diagram of a metal-semiconductor system:
(a) before contact, (b) after contact.

one can image the spatial variation of the electronic properties of the metal-semiconductor interface. For example, Kaiser et al. have found that the Au-Si interface is spatially homogeneous, whereas the Au-GaAs interface shows heterogeneity on a lateral scale of 2 nm.[16,19]

The BEEM also has been used successfully in measuring many different properties of the metal-semiconductor system such as Schottky barrier heights, interface transport, and conduction band structure.[20] Further, by using positively-biased tips and p-type semiconductors, ballistic hole spectroscopy has been performed, giving information on the valence band.[21,22]

Besides the metal-semiconductor systems, the BEEM can be used, in principle, to investigate the metal-vacuum interface. This feasibility is mentioned briefly in Ref.16. The basic idea is very simple. Instead of having a base of thin metal on the semiconductor substrate, now the base is a thin free-standing metal film in a vacuum. An STM tip injects electrons into the base, and some of these electrons reach the back of the film without any energy loss. If these electrons have enough energy to climb the potential step (or work function) at the metal-vacuum interface, some fraction of them will leave the metal and will go into the vacuum. These electrons can be collected and the current due to them, which is the collector current, can be measured.

The BEEM adaptation for the metal-vacuum interface, that is described above, can be used for many different types of

studies. For example, by measuring the threshold voltage at which the collector current begins, one can measure the work function of the metal surface. This is a new technique for measuring metal work functions. A striking feature of this new technique is that it uses only a very small area (less than 100 nm^2) of the sample at a time. Therefore this method can yield work functions with high spatial resolution. The work function is an important parameter of metals that has been measured through the use of several different techniques. For example, the work function can be obtained from the measurement of thermionic emission current vs. temperature, the measurement of photoelectric yield as a function of the incident photon energy, the measurement of contact potential difference against a suitable reference, and the measurement of field emission current as a function of applied electric field. Different measurements of work function values tend to vary somewhat. For example, Ashcroft and Mermin[23] list the preferred value for the work function of polycrystalline gold as 4.3 eV, while the 1992-1993 edition of the Handbook of Chemistry and Physics lists that as 5.1 eV.[24] Further, many of these measurements are spatially averaged values over the samples. Therefore, another independent method of measurement of work functions, with high spatial resolution, should be useful. By performing a raster-scan of the sample with the injecting tip, the BEEM will be able to map out spatial variations of the work function that can arise from crystal defects or adsorbates on the surfaces. It is

particularly interesting to see how the work function varies over the surface as a clean metal surface is progressively covered with adsorbates.

Further, by the energy analysis of the emitted electrons, one can obtain information about scattering processes, such as plasmon excitations that can take place in the base. Also, in the same manner, one can study the excitation of molecules adsorbed on the surface. All these can be done with considerably high spatial resolution.

It may appear that the STM is the ideal tool to investigate the work function variations due to adsorbates and crystal defects. This is because, according to the simple theory, the tunnel current I in the STM is given by Eq. 1, where ϕ is the average work function of the tip and the sample. Thus, from the variation of the tunnel current when the tip is moved towards (or away from) the sample, the value for ϕ can be extracted. However, the work function values that are measured by STM's are way below the accepted work function values, except for a few measurements done in ultra clean conditions.[25,26] For example, when the STM is used in air and even in low vacuum (10^{-7} torr), it is typical to get an apparent value of ϕ in the range of 0.5 eV - 1 eV for metals whose work functions are about 4 eV.[27,28] The expected work function value for gold is about 5 eV. This fact alone rules out the STM as a meaningful tool for the study of work functions. Further, there exists a huge electric field between the tip and the sample. For example, in an STM with a

100-mV bias and a 1-nm tip-sample spacing, a field of about 10^8 V/m exists between the tip and the sample. (As a comparison, electric breakdown occurs in air at an electric field of about 3×10^6 V/m.) This strong field may have profound effects on the STM measurements on adsorbates. Apart from electric fields, the presence of the STM tip brings about strong forces of interaction in the tip-adsorbate-substrate system. Pressures in the range of giga-Pascal have been estimated.[29] Pressures of these magnitudes are expected to affect electronic properties of the adsorbates.[30] Thus, even though the STM is superior in topographic imaging, there clearly are situations where the study of surface properties calls for a technique in which the tunnel tip is remote from the point of study.

Despite the apparent simplicity of applying the BEEM to the metal-vacuum interface, this type of study has not yet been performed successfully. There are considerable difficulties to be overcome. One of the major difficulties is the preparation of very thin free-standing samples. It is not even known whether an STM can operate over a free-standing film of thickness of a few tens of nm.

The aim of this present work is to investigate experimentally the process of ballistic electron emission into the vacuum through thin free-standing films. Since no one has performed the techniques of the BEEM on free-standing thin films, this dissertation will emphasize on the preparation and characterization of free-standing thin films. We will prepare

free-standing Au films of different thicknesses under different conditions. We will characterize these films using optical microscopy, electron microscopy, and the STM. We will report ballistic electron emission spectra that are obtained on selected films. We will also obtain an upper limit for the value of the work function for the gold films under the given conditions. In the rest of this thesis, we will describe the details of our efforts and the results obtained. Some future directions are also being suggested. We will report our efforts on using the ballistically emitted electrons for the purpose of imaging the thin films.

This dissertation is arranged as follows. The description of the equipment is in Chapter II. Chapter III describes the sample preparation and characterization. The results of the ballistic electron emission experiments is presented in Chapter IV, and finally the conclusions of our study is given in Chapter V.

CHAPTER II

EQUIPMENT

We designed and constructed a novel experimental set-up in order to apply the BEEM configuration to a metal-vacuum interface. The schematic diagram of the set-up is shown in Fig. 4. This set-up consists essentially of an STM in a high vacuum ambient, a thin free-standing metal film (base) that acts as the sample for the STM, and a channel electron multiplier (CEM). In the following we describe the equipment in detail.

The experimental configuration is shown in Fig. 5. We constructed the STM by first gluing a piezoelectric scanner onto a precision XYZ translator (Newport Research MT-XYZ). The translator is driven by 80-pitch screws. The translator has an ultimate resolution of 1 μm, and a range of 6 mm in all the three directions. We secured the multi-axis translator onto the stainless steel base plate. (See Fig. 5.) The piezoelectric scanner is made of a radially polarized piezoelectric tube. The inner and the outer surfaces of the tube have metal electrodes
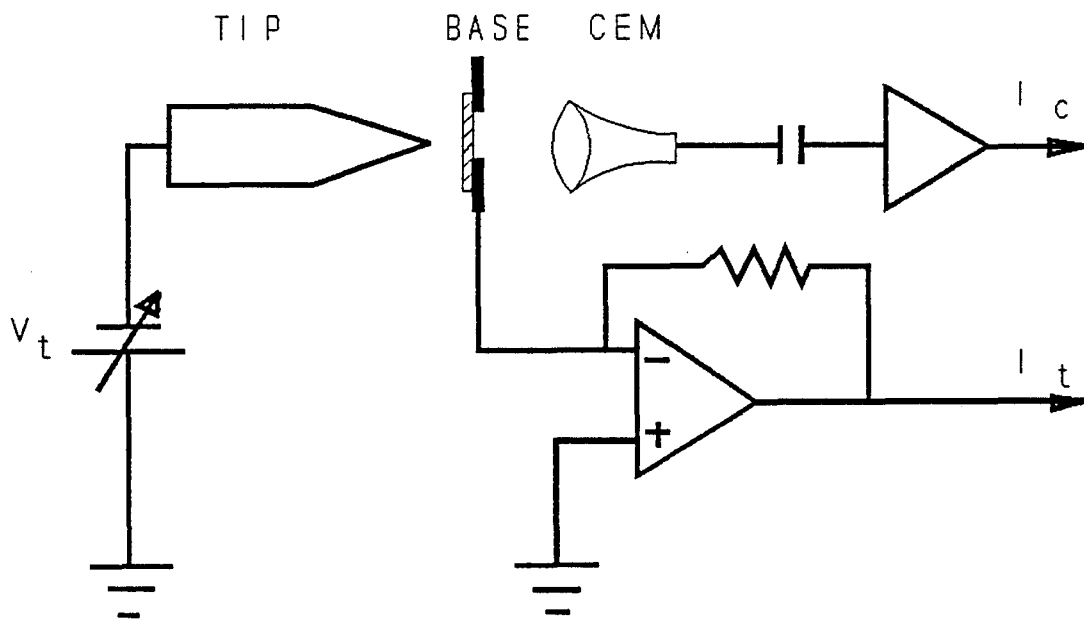
FIG. 4. Schematic diagram of the experimental set-up for BEEM to investigate metal-vacuum interface.

MULTI-AXIS TRANSLATOR

CHANNEL ELECTRON MULTIPLIER

SAMPLE

BI MORPH

Piezoelectric tube

STAINLESS STEEL BASE PLATE
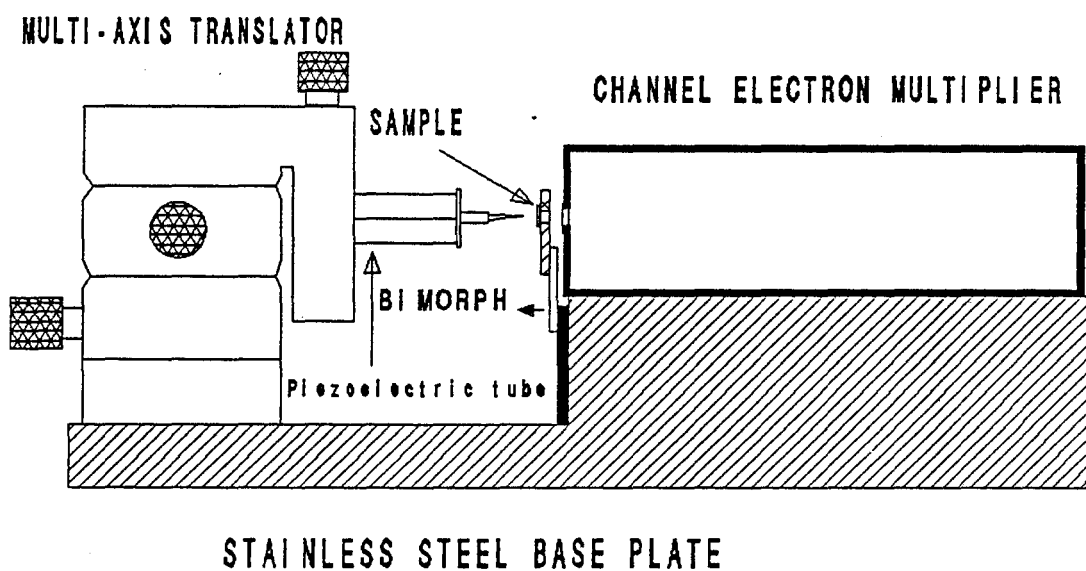
Fig. 5. Ballistic electron emission microscope (BEEM) used to investigate metal-vacuum interface. All components of the BEEM are UHV compatible.
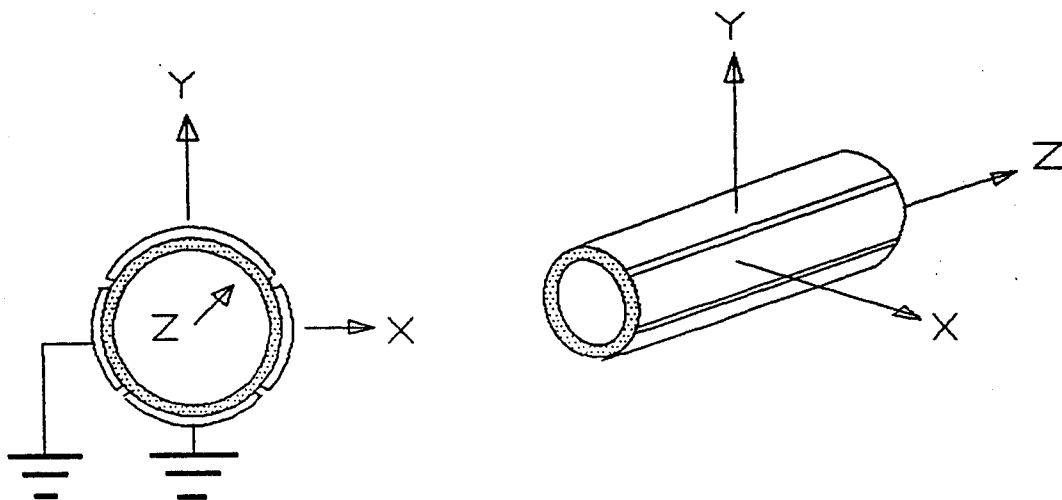
FIG. 6. Piezoelectric tube scanner. Piezoelectric material is sandwiched between inner and outer electrodes. Outer electrode is segmented lengthwise into four quadrants.

that are deposited on them. Binnig et al. showed how to construct a scanner in three dimensions by using a single piezoelectric tube.[31] According to their design, which we followed, the outer electrode is segmented lengthwise into four equal quadrants as shown in Fig. 6. The inner electrode is used to obtain motion in the direction normal to the sample (the Z direction.) For example, when the voltage of the Z electrode (that is, the inner electrode) is changed, the length of the tube will change accordingly. On the other hand, when the voltage of an outer electrode is changed while keeping others constant, the length of that particular section of the tube will have to change. This causes the tube to bend, and this bending is used to achieve motion in the X-Y plane. A pair of outer electrodes that are placed 90° apart are used to obtain the motion in the X-Y direction. The other pair of the outer electrodes is kept grounded.

We glued one end of the piezoelectric tube to the translator as shown in Fig. 5. We used a tube that has a length l equal to 1.27 cm, and an inner radius r_i equal to 0.254 cm, and an outer radius r_o equal to 0.305 cm. The scanner has a maximum range of about 1 μm in each dimension, for an applied voltage of $\pm$ 100 V.

The lowest resonance frequency f_r (in Hz) of the scanner, that corresponds to the bending mode, is estimated from the following equation:

$$f_r = 1.08 \times 10^5 \left[\frac{\sqrt{r_0^2 + r_i^2}}{l^2} \right] \; Hz \qquad (3)$$

In the above equation the lengths are in cm. The lowest resonance frequency is estimated to be 26.5 kHz.[2] We mounted the tip on a tip holder that is glued to the other end of the piezoelectric tube. The tip holder consists of a stainless steel tube of 0.3-mm inner diameter that is attached to a stainless steel disc. (See Fig. 7). The tube passes through the center of the disk. The tip, which is made of a wire of a diameter less than 0.3 mm, goes into the tube such that the sharp end of the tip sticks out. We secured the tip in the stainless steel tube by the spring action of another wire that presses on the tip through a slit on the side of the tube.

We also utilized a piezoelectric bimorph to aid in the tip-sample (base) approach, since it was difficult for us to adjust distances in steps smaller than about 10 μm by using an 80-pitch screw. A piezoelectric bimorph consists of two piezoelectric strips that are glued on top of each other such that their directions of polarizations face opposite directions. Thus when a voltage is applied across such a bimorph, one strip expands while the other contracts resulting in a bending motion. By using bimorphs, one can easily obtain large range motion (of the order of 100 μm), with small voltages (less than 100 V). The
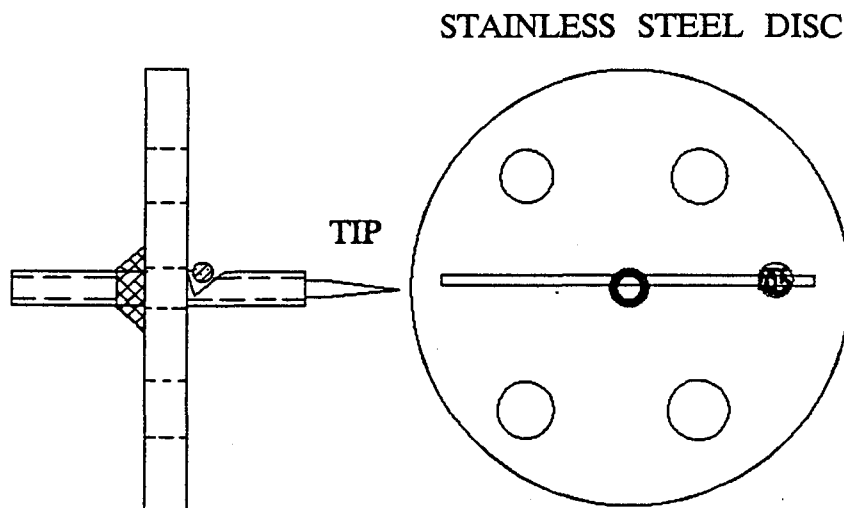
STAINLESS STEEL DISC

TIP

FIG. 7. The tip and stainless steel tip holder.

bimorph that we used has dimensions of 6.25 mm x 12.5 mm x 0.5 mm, and yielded a range of motion of about 30 μm with an applied voltage range of ± 50 V. The bimorph was attached at one end to a small stainless steel plate (see Fig. 8), which in turn is secured onto the base plate with screws. The free part of the bimorph, l_c, is 0.35 inch. The resonance frequency f_r (in Hz) of this bimorph configuration can be obtained as 2857 Hz, by substituting l_c (in inches) in the following equation.[32]

$$f_r = \frac{350}{l_c^2} \tag{4}$$

The sample holder, which is a small aluminum piece, with a hole at the center, is attached to the other end of the bimorph so that the hole sticks out. The sample, which is a thin metal film supported on a Cu grid, is attached to the sample holder so that the central part of the sample is over the hole. The necessary electrical connections to the piezo-elements are done by attaching wires with silver paint.

To measure the collector current, we use a channel electron multiplier (CEM) instead of an electrometer used in regular BEEM experiments.[16] This gave us the ability to measure very small currents since with the CEM one can count a single electron at a time, whereas with a typical electrometer, it is difficult to measure current smaller than 1 pA. A CEM is a narrow glass tube (usually curved) whose interior is coated with a material of high electrical resistance. One end of the tube is at a low

SAMPLE   UHV EPOXY   ALUMINUM PIECE   BIMORPH
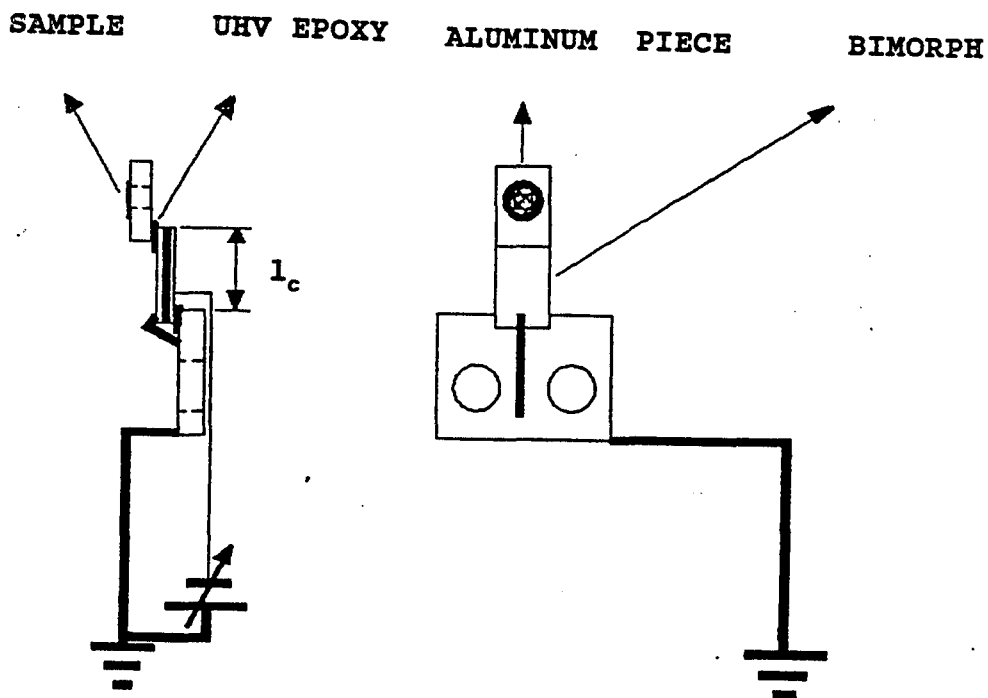
l_c

FIG. 8. The bimorph is attached to a stainless steel piece which is mounted onto the stainless steel base plate. The small aluminum piece which has the sample on it is attached onto the bimorph. Silver paint is used for electrical conductions between lead and the material.

potential (eg. 100 V) while the other end is at a high potential (eg. 3 kV). An electron entering the low voltage end gets accelerated by the low voltage and hits the wall of the tube at some point, generating several secondary electrons. These secondary electrons get accelerated and hit the tube wall somewhere down the tube generating more secondary electrons. This process continues down the tube, ultimately building an avalanche of electrons. A single electron entering our CEM can typically generate more than 5×10^7 electrons. This electron pulse is converted to a voltage pulse using a charge sensitive preamplifier.

We used a commercially available, complete CEM detector system (Amptektron model MD-501) in which, the CEM, the high voltage supply, the preamplifier and discriminator, and the electronics are packed into one compact unit. This unit is placed directly in the vacuum chamber and is powered by a +15 V supply. The detector system outputs a voltage pulse for a low-energy (a few eV) electron entering it. These pulses are of fixed maximum height of 5 V and of duration of 220 ns. These pulses are counted by using a counter on our data acquisition card (Scientific Solutions, Inc., Labmaster card) that is plugged into a microcomputer. This counter counts TTL logic (0V - 5V) pulses. The computer is programmed to read the counter at preset time intervals. Our detector has a typical dark current of 0.1 counts/sec and a maximum rate of counts of over 10^6 counts/sec. We also have a commercial frequency counter (BK

Precision model 1805) which continuously displays the rate of counts.

As our experimentation is to be performed in vacuum, we put together an ultra high vacuum system. The set up is shown in Fig. 9. The UHV chamber, which is made of stainless steel, consists of 6 ports of 8-inch flange and 10 ports of 2.75-inch flange. One 8-inch port and five 2.75-inch ports have glass view ports on them for the purpose of viewing the inside of the chamber. The chamber is pumped at higher pressures (greater than 10^{-2} torr) by using either cryogenic sorption pumps or a turbo molecular pump. To achieve lower pressures, a 270 l/s ion pump is used. A UHV gate valve is placed between the chamber and the ion pump. This enables us to open the chamber to the atmosphere with the ion pump continuously working. Heating elements are attached to the chamber as well as to the ion pump for baking out the system. With this system, we have achieved about 1 x 10^{-9} torr pressures. However, with the CEM inside the chamber, the lowest pressure is limited to about 2 x 10^{-8} torr. The chamber is equipped with a residual gas analyser (RGA) that can give partial pressures of the constituents of the vacuum. The whole system is placed on four vibration-isolating air legs (Barry STABL-LEVL-SLM 3A).

We tested our UHV STM by imaging a 300 nm thick Au film on a mica substrate. The imaging was done at a pressure of about

UHV GATE VALVE

CHAMBER

ION PUMP

ADSORPTION PUMP
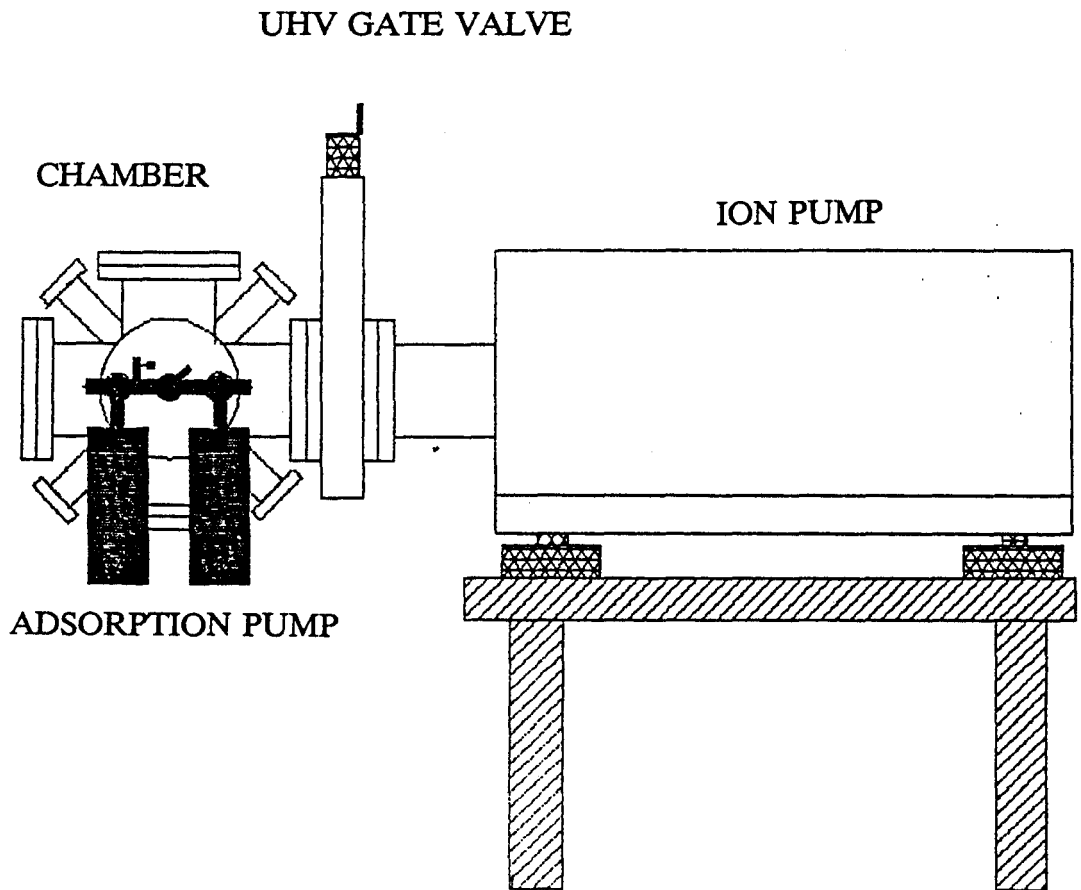
FIG. 9. Schematic diagram of UHV BEEM system to investigate metal-vacuum interface.

1×10^{-9} torr. The images are shown in Fig. 10. The images are of satisfactory quality. However, as we have incorporated a low frequency (a few kHz) component (the bimorph) in the STM design, we cannot expect atomic resolution from this STM. With noise coming from our ambients, we can obtain a resolution of about 1 nm. This is satisfactory for our experiments since we do not expect (at this stage) to perform experiments at any higher spatial resolution with BEEM.

(a) (b)

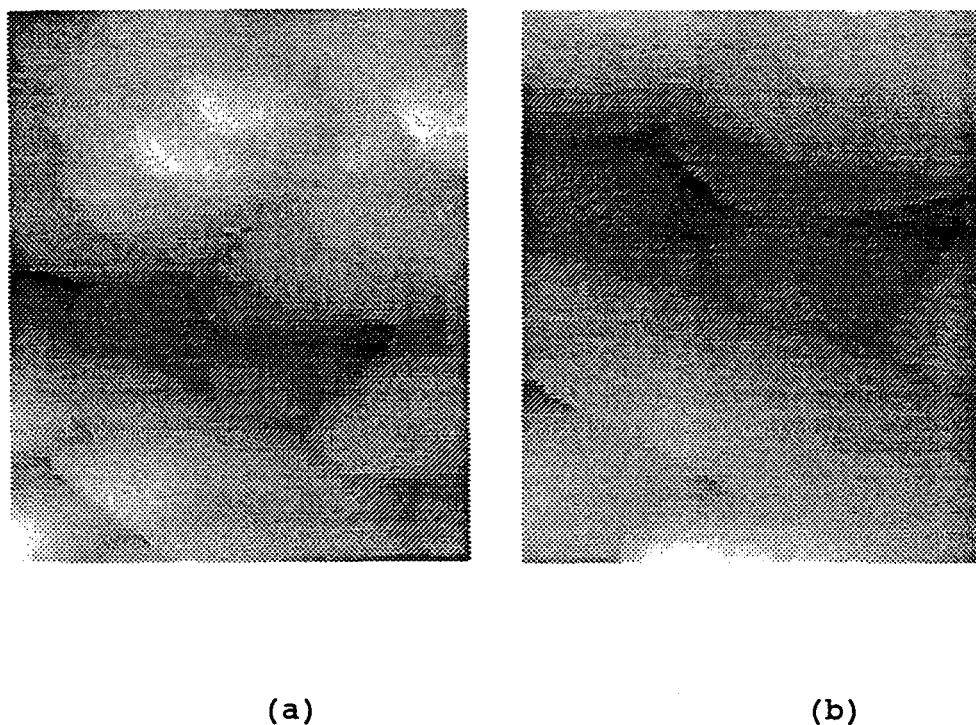FIG. 10. STM topographic image of a 300-nm thick gold film on mica. This image was obtained at 10^{-9} torr UHV pressure and at room temperature. The applied bias voltage between the tip and the sample is V_t=-0.125 V, and the tunneling current is I_t=0.2 nA.

(a) Scan area, 65 nm x 65 nm and height variation, 33 nm.

(b) Scan area, 30.6 nm x 30.6 nm and height variation, 33 nm.

CHAPTER III

PREPARATION OF THIN, FREE-STANDING METAL FILMS

FOR THE BALLISTIC ELECTRON EMISSION EXPERIMENTS

Kaiser et al., in their ballistic electron emission microscopy of metal-semiconductor interfaces, used a metal film of about 10 nm thick as the base. This base can be obtained easily by evaporating a metal film of required thickness onto the semiconductor. Such films give collector currents of the order of pico-Amperes for one nano-Ampere injection currents when the tunnel bias exceeded the Schottky barrier height by a few tenths of a volt.[16] For the present work, what we need is such films in an unsupported form. The successful preparation of such free-standing metal films that are thin enough to give a reasonable transmission, and yet strong enough to withstand the STM experimentation is crucial to the present work.

The thinner the base, the larger the collector signal will be. However, the base will be more fragile. We can measure collector currents as small as a few electrons per second with the use of the channel electron multiplier (CEM). Our CEM has

a dark-current of about 0.1 counts/sec. Thus we can somewhat relax the thickness requirement of the base in the present experiment compared to that of the metal-semiconductor experiment of Kaiser et al.[16] We can estimate the maximum base thickness that can be tolerated as follows. The collector current consists of electrons whose energies (in the base) are slightly above 5 eV (relative to the Fermi level). For 5-eV electrons, the mean free path l in a metal such as gold is about 4 nm.[33] If the tunnel current is I_t, and the base thickness is t, then the electron current that impinges on the back surface of the base, due to the electrons that did not suffer any energy loss, is I_t exp(-t/l). If we take the transmission factor for the barrier to be 0.5 and the detector efficiency of the CEM to be 0.5, then the detected collector current is 0.25 x [I_t exp(-t/l)]. Thus if we demand that the detected collector current should be at least 100 electrons/second, while the injection current I_t is 1 nA, then the maximum value of t is about 65 nm, which is a fairly thick film. However, the spatial resolution of the BEEM measurement goes down with the thickness of the base.[34] Therefore, in order to have a higher signal as well as better spatial resolution, the base thickness should be made as thin as possible. We have experimented and established a procedure that has yielded high quality, free-standing thin films of thicknesses down to 17 nm. In the following, we describe the details of our efforts and the characteristics of our films.

In order to produce thin, free-standing films, we briefly tried electrochemical etching, and ion milling of thin foils. Later, we gave up these methods in favor of evaporation onto removable substrates, which is one of the sample preparation techniques used in transmission electron microscopy (TEM). In the procedure that we have followed, Au of the desired thickness was thermally evaporated onto cleaved NaCl crystal substrate of (100) orientation. Au is known to grow in (111), and (100) orientations on (100) face of NaCl even at very low coverages.[35] The pressure during evaporation was in the low 10^{-6} torr region. The thickness was controlled with a quartz thickness monitor during the evaporation. The thin film was removed from the NaCl substrate by dissolving the substrate in distilled water. The thin film which floated on the surface of the solvent was caught onto a grid which acted as the support for the thin film. The commercially available Cu grids that are used in TEM were found to work well. For very thin films (less than 20 nm thick), the surface tension of the water seemed to break up the film while the grid was pulled out of the water. We alleviated this problem by using as the solvent a 50-50 mixture of ethyl alcohol and distilled water. The surface tension of this mixture is smaller than that of pure water by a factor of about 2.42.[36]

In our initial attempts, we kept the NaCl substrate at 77 K during the evaporation. Jaklevic et al. have demonstrated that very thin continuous Au films can be deposited on such cold

substrates.[37]   These films were mounted on the grids as described above. Under an optical microscope, the free-standing films appeared fine.   To further characterize these films in high resolution, we used electron microscopy. Figure 11 shows a TEM picture of a 17-nm thick, free-standing gold film prepared this way. We can see that the film contains many ruptures and holes. Thus this film is not of a quality that is suitable for our experiment. For example, when the tip approaches the sample, there is a good possibility that the tip will be located over a hole.   This situation can give rise to unpredictable results including further damage to the film due to the pushing tip.   Another problem that is associated with our samples is seen also in Fig. 11.   The darker patches seen, we believe, are residues from the NaCl substrate.

The electron diffraction pattern obtained for this film is shown in Fig. 12. The electron beam spot had size of 0.2 μ in diameter. The camera constant (wavelength x camera length) used was 0.001 nm.m. We indexed the first few rings in the pattern (in the order of increasing diameter) as (111), (200), (220), (311), and (222) planes of Au, respectively. It should be noted that the last two of the above rings ((311) and (222)) are very close to each other. The rings of the diffraction pattern indicate that there are many randomly oriented crystallites within the 1 μ-diameter spot. This film is not a satisfactory

FIG. 11. Transmission Electron Micrograph of a 17-nm gold thin film. The film was prepared by evaporating Au onto (100) face of NaCl, at 77 K. Darker patches are believed to be the residues of NaCl on gold thin film.
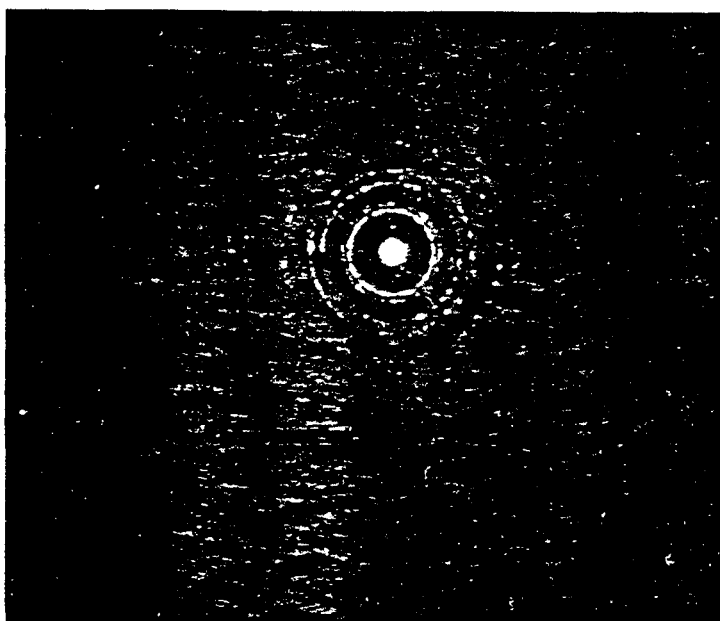
FIG. 12. Diffraction pattern of the 17-nm thick gold thin film, that was prepared by evaporating onto NaCl substrate at 77 K.

crystal quality for our experiments. There is a good possibility that the tip will tunnel onto an area of high disorder where the electron mean free path may be small.

Learning from the above results, we modified the procedure of sample preparation. Now, we prepared thin films by evaporation onto substrates that were at room temperature. Also, the films were washed for a second time to reduce the residual NaCl. Figure 13 shows a bright field TEM picture of a 24 nm-thick free-standing Au film that was prepared in this manner. As can be seen, the film is free of holes and ruptures and the grains can be seen clearly. Also the dark patches of residual NaCl are missing. In order to improve crystal quality, we annealed the free-standing films. Figure 14 shows a 24 nm-thick film that was annealed at 450 K for 20 minutes. The grains have grown bigger. Figure 15 shows a diffraction pattern that was obtained on a particular grain of an approximate size of 0.7 μ of that film. The camera constant used was 0.002 nm.m. From the symmetry and the separation of the spots, we identify that the grain is (111) oriented and the spots are due to {022} planes. A large number of such (111) oriented grains were seen. This film is satisfactory for our application since the grain sizes are comparable to the maximum scan size of the STM, and are much larger than film thickness. We expect that we will be able to perform our BEEM measurements on a single grain at time, away from grain boundaries.
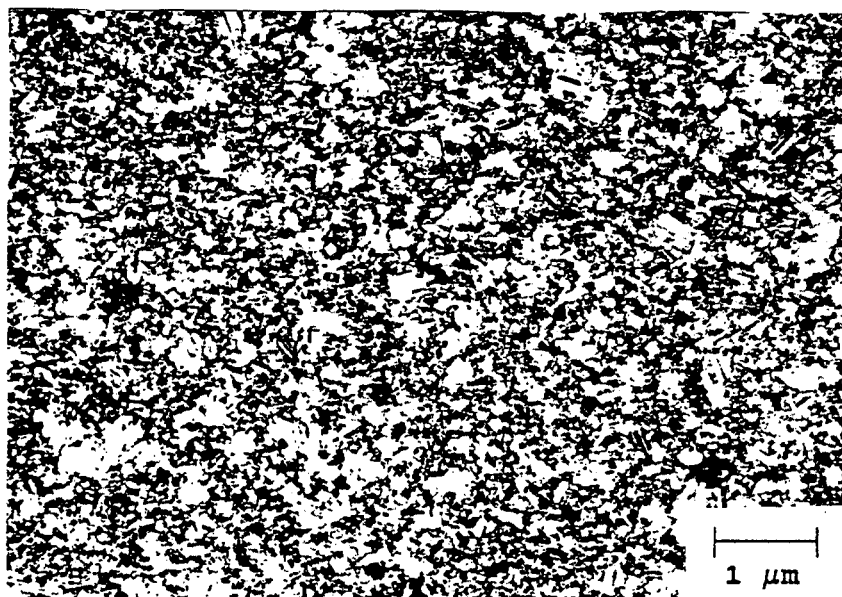
FIG. 13. Bright field TEM image of a 24-nm thick gold film. The film was prepared by evaporating Au onto (100) face of NaCl at room temperature.
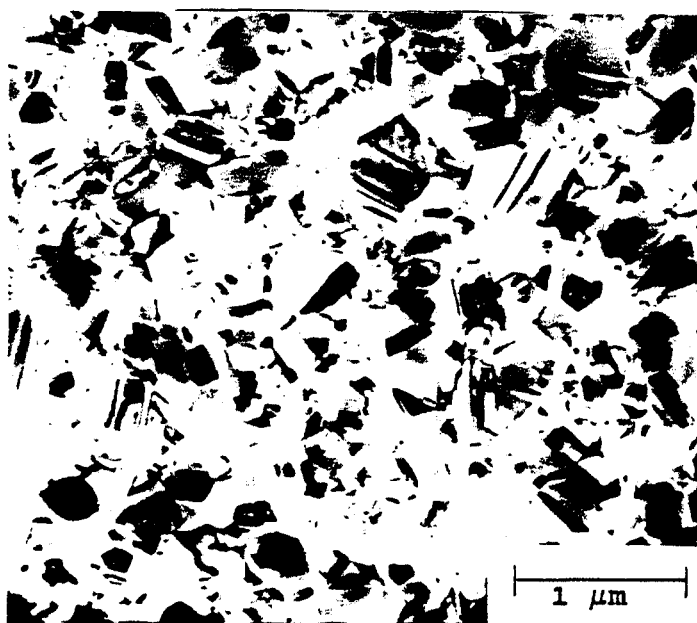
FIG. 14. Bright field TEM image of a 24-nm thick annealed gold film.

FIG. 15. Diffraction pattern obtained on a particular grain of
a 24-nm thick gold film.

An added benefit of annealing is the improvement of the bonding between the Au film and the Cu grid. This bonding was evident from the fact that when the sample was dipped in the water after annealing the film, the film and the grid did not separate, whereas before annealing, they did. In order to monitor the annealing process, we assembled a high-vacuum annealing station where the sample can be viewed through an optical microscope while the annealing proceeds. Most of the wrinkles that may be present on the thin film after the thin film is caught onto the grid disappear while annealing at the appropriate temperature.

Thus, this procedure - of evaporating a thin Au film on a NaCl substrate at room temperature, dissolving the substrate in a mixture of alcohol and water, catching the film onto Cu grids, and annealing - seems to produce satisfactory samples for our experiments. Figure 16 shows STM topographs of some free-standing thin films.
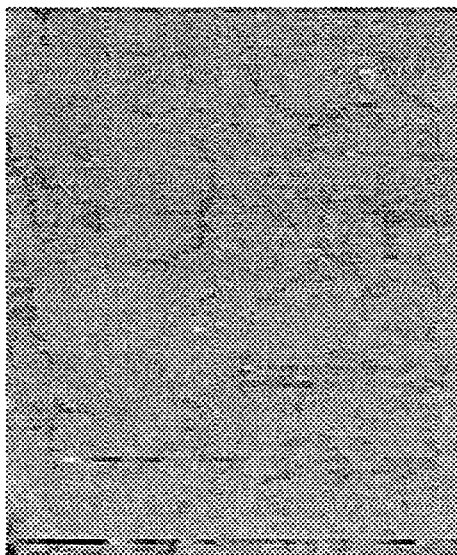
FIG. 16. STM topographic image of an unannealed 40-nm thick free-standing gold thin film. This image was obtained at 10^{-7} torr pressure and at room temperature. The applied bias voltage is $V_t=-1.279$ V and the tunneling current is $I_t=0.6$ nA. The scan size is 250nm x 250 nm. The height variation is 8.7 nm.

CHAPTER IV

BALLISTIC ELECTRON EMISSION FROM AN STM TIP

INTO VACUUM THROUGH A THIN GOLD FILM

We have studied the process of ballistic electron emission over the metal-vacuum barrier with our experimental set-up. We have used free-standing Au thin films of various thicknesses that we prepared as described in the previous chapter. We formed the tips by the electro-chemical etching of 0.25 mm-diameter gold wires in hydrochloric acid. We mounted the sample on a holder at the end of the piezoelectric bimorph. We brought the tip to the tunneling range of the bimorph by using the precision translator. Then, we applied the needed voltage to the bimorph to bring the tip-sample spacing down to the tunneling range. The tip approach was done in air. Once the tip was in the range of the bimorph, we loaded the STM into the vacuum chamber and we pumped down the chamber. We performed ballistic electron emission experiments in high vacuum.

In order to perform the ballistic electron emission experiment, first, we obtained a tunnel current of about 1 nA with a tunnel bias (the tip was negative) of about 0.1 V. Then, we ramped up the tunnel bias up to about 10.5 V in 128 equally spaced voltage-steps. During this ramping, the tunnel

current was kept constant by the feedback loop of the STM. At
each bias voltage value, we counted the pulses from the CEM for
a period of 10 msec. (This rate of counts gives the collector
current at that bias voltage.) At the end of the ramping up,
the bias voltage was ramped down, again with the collector
current being monitored.

Some typical results that we obtained for a 40 nm-thick
annealed gold film are shown in Figs. 17-22. Each data point
was obtained by counting the output pulses from the CEM for 10
msec. Each curve consists of 128 data points. Thus the time
needed to measure one curve (ramping up or down) was about 1.3
s. As can be seen in the figures, the behavior is quite diverse.
In Figs. 17-19, the collector current starts at a bias of about
5 V, which is what can be expected since the work function of
gold is found in the literature to be 4.8 - 5.2 eV.[24,21]
However, the collector current does not stay steady and tends to
decay towards low values very rapidly. For example, in Fig. 18
the collector current decayed to zero by the time the tunnel
bias reached the value of about 10 V. The collector current
stayed near zero value throughout the ramping down for this
particular case. The decay of the collector current made
ramping up and ramping down curves different. Also, we could
not have a collector current over any extended time period. As
can be seen in Figs. 17-22, the threshold voltage for the start
of the collector current varied between 5 V and about 10 V. In
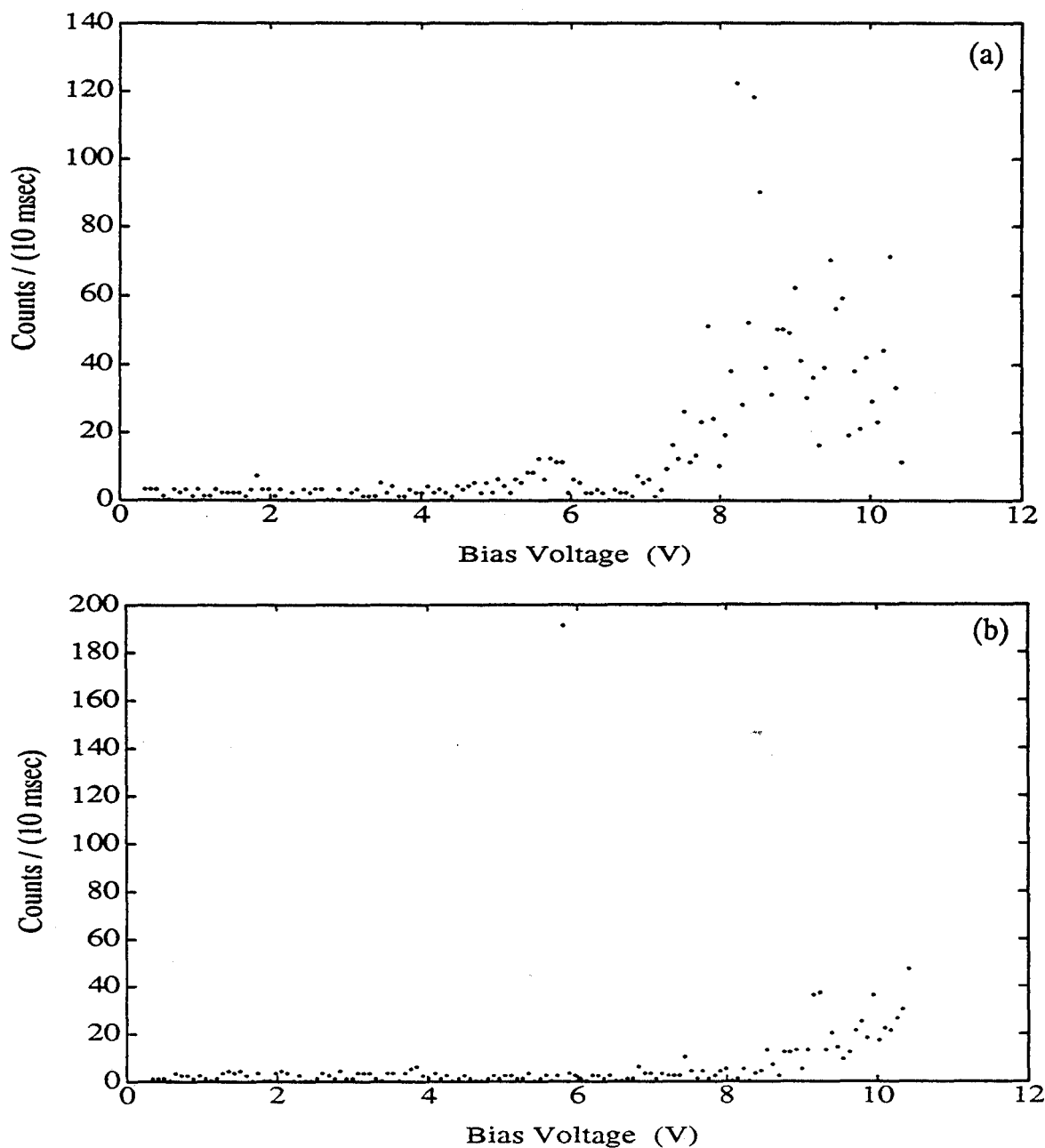fact, there were many curves with threshold voltages greater

FIG. 17. The plot of the collector current versus the bias voltage. The bias voltage was swept from 0.293 Volts to 10.5 Volts. The data was taken at room temperature, 10^{-8} torr pressure, and with coordinates x = 25, and y = 25. (a) Upward bias voltage motion. (b) Downward bias voltage motion.
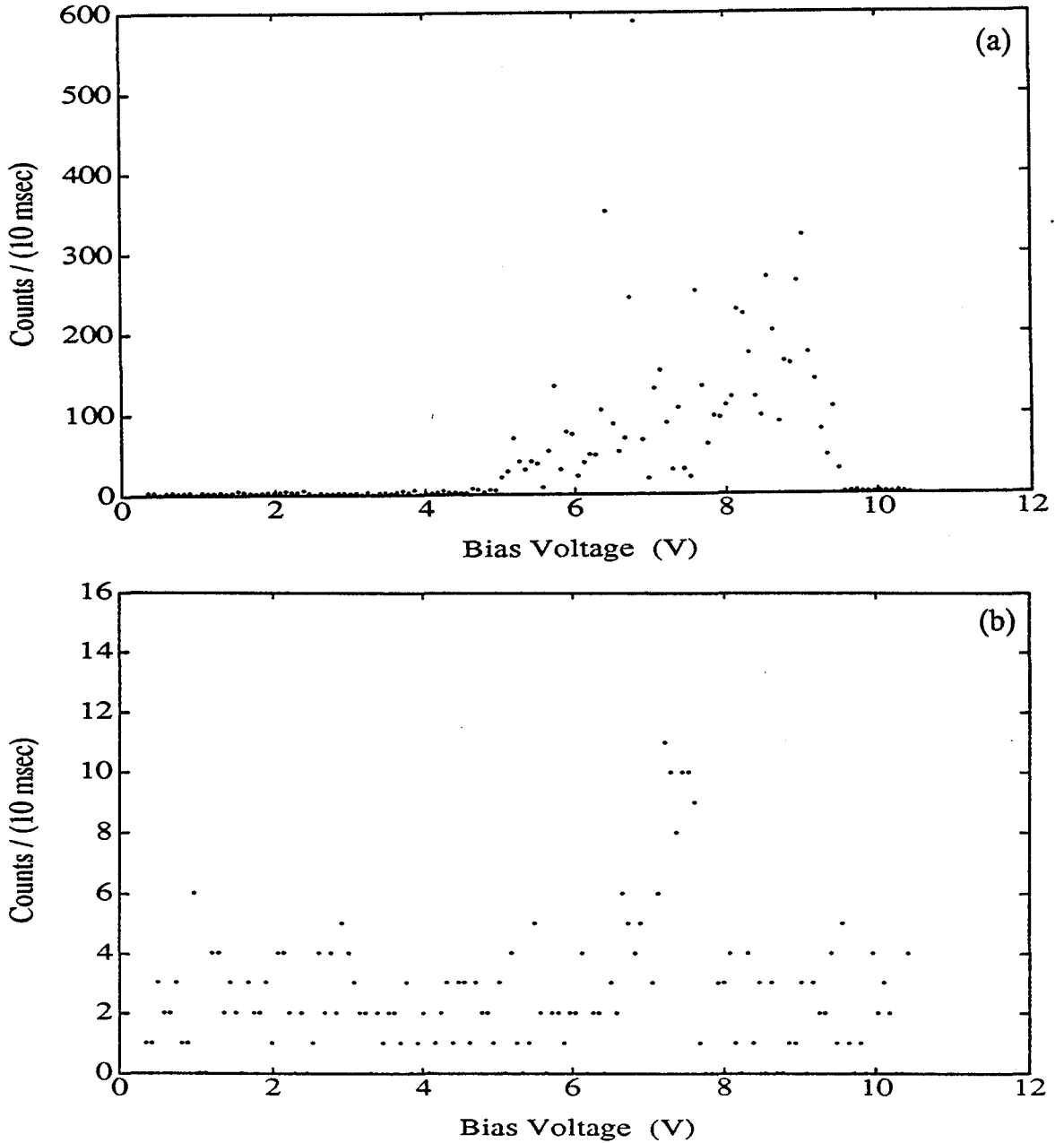
FIG. 18. The plot of the collector current versus the bias voltage. The bias voltage was swept from 0.293 Volts to 10.5 Volts. The data was taken at room temperature, 10^{-8} torr pressure, and with coordinates x = 25, and y = 25. (a) Upward bias voltage motion. (b) Downward bias voltage motion.

FIG. 19. The plot of the collector current versus the bias voltage. The bias voltage was swept from 0.293 Volts to 10.5 Volts. The data was taken at room temperature, 10^{-8} torr pressure, and with the coordinates x=100, and y=60. (a) Upward bias voltage motion. (b) Downward bias voltage motion.
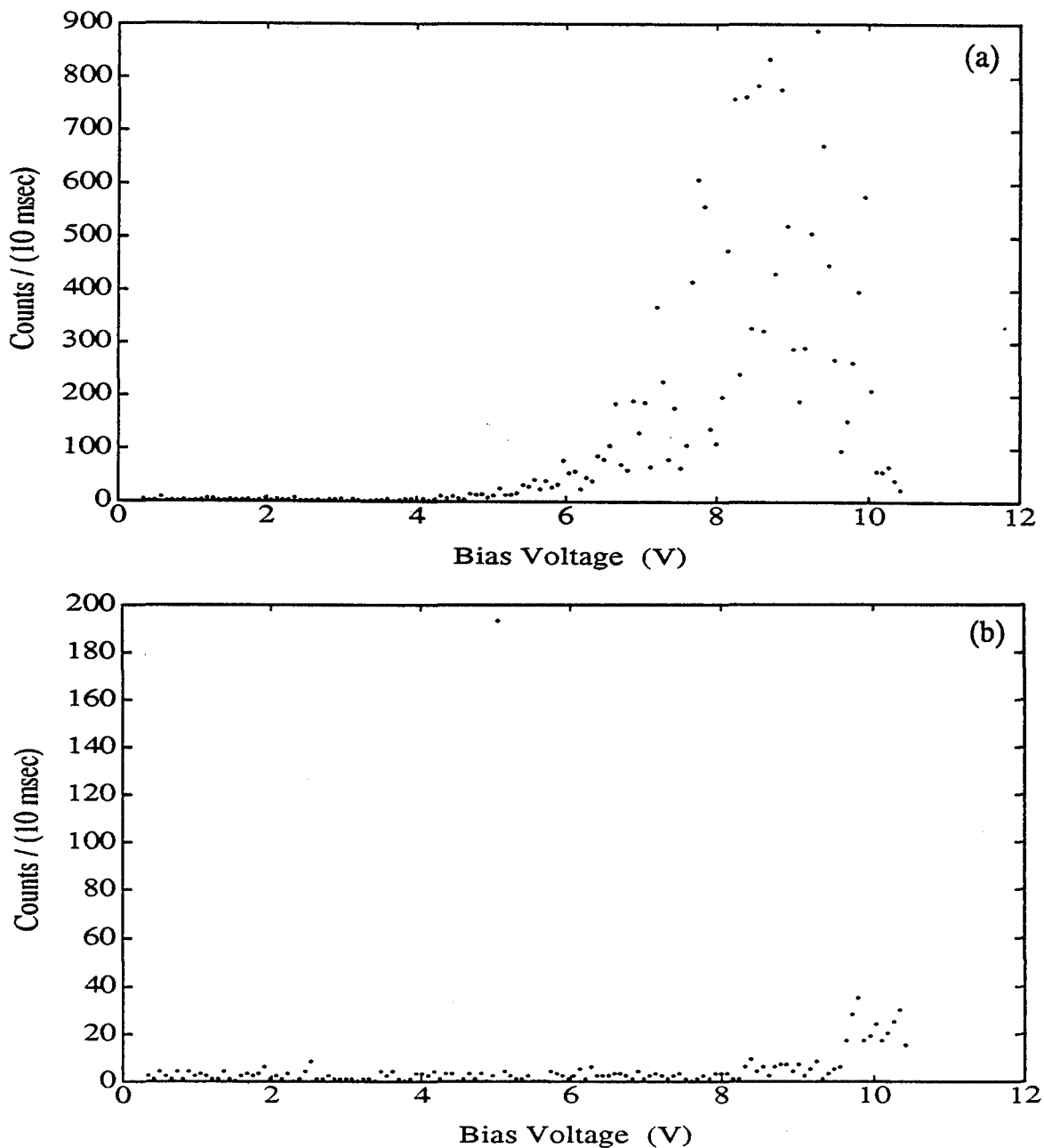
FIG. 20. The plot of the collector current versus the bias voltage. The bias voltage was swept from 0.293 Volts to 10.5 Volts. The data was taken at room temperature, 10^{-8} torr pressure, and with coordinates x = 100, and y = 100. (a) Upward bias voltage motion. (b) Downward bias voltage motion.
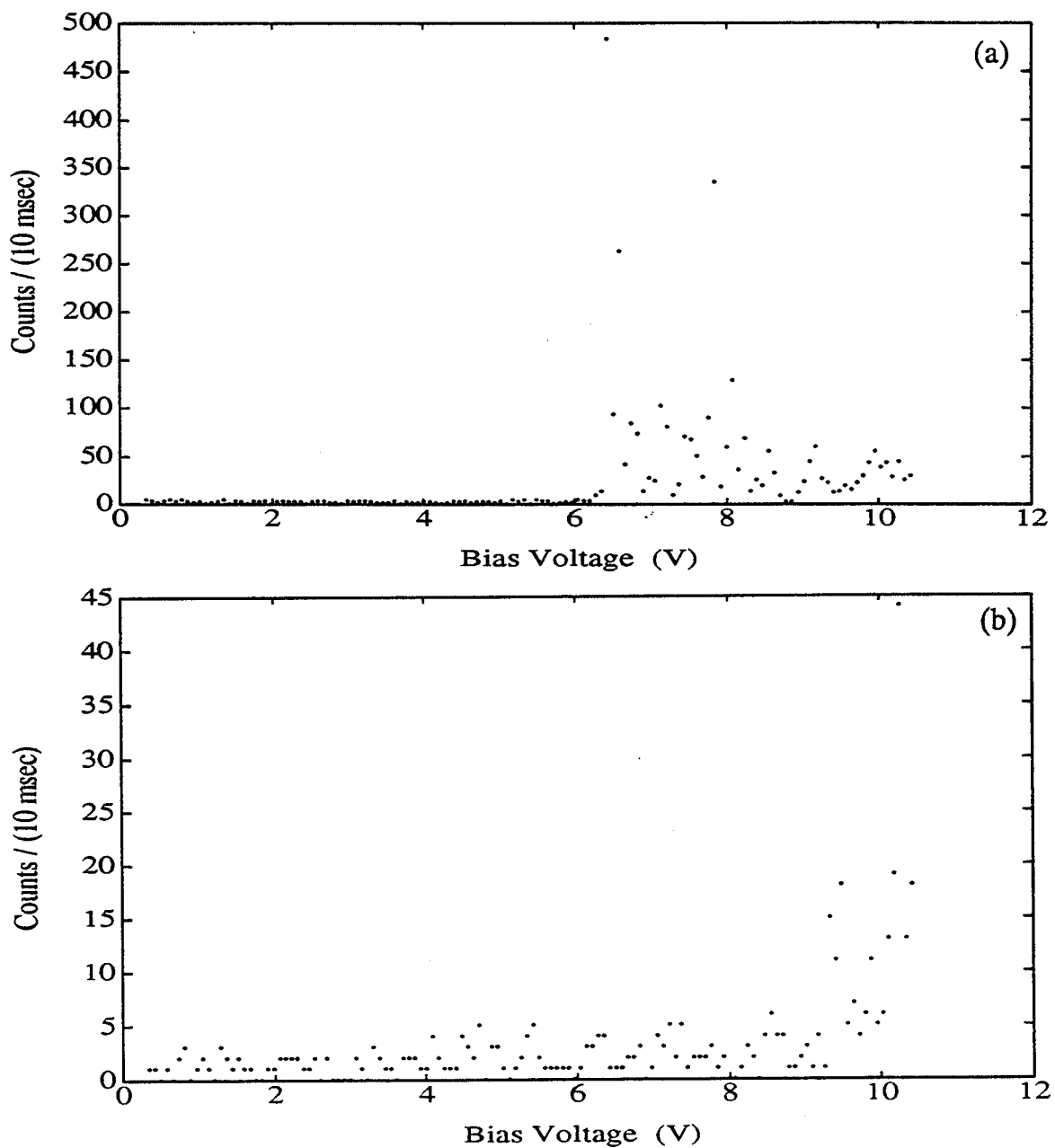
FIG. 21. The plot of the collector current versus the bias voltage. The bias voltage was swept from 0.293 Volts to 10.5 Volts. The data was taken at room temperature, 10^{-8} torr pressure, and with coordinates $x = 75$, and $y = 75$. (a) Upward bias voltage motion. (b) Downward bias voltage motion.
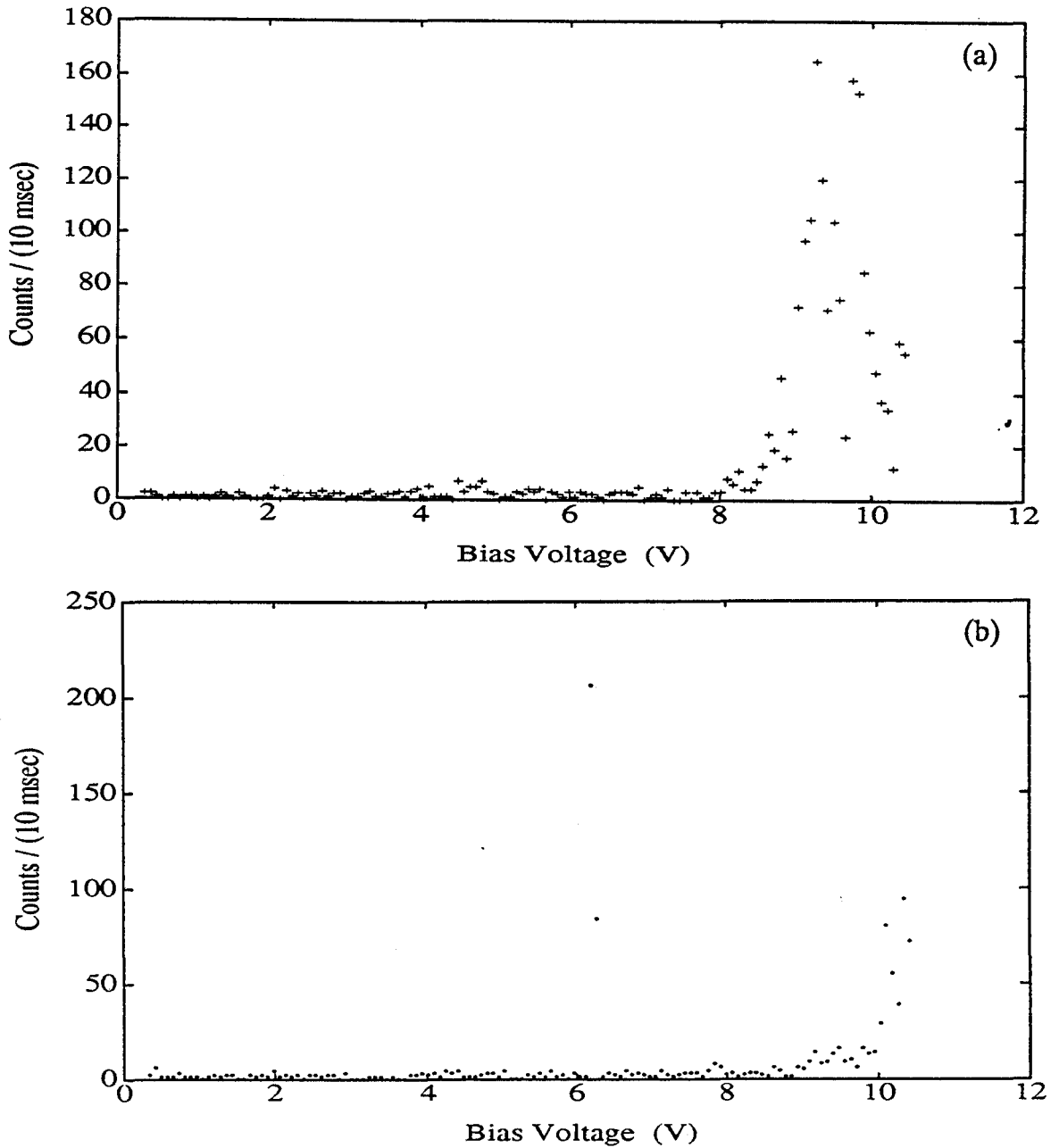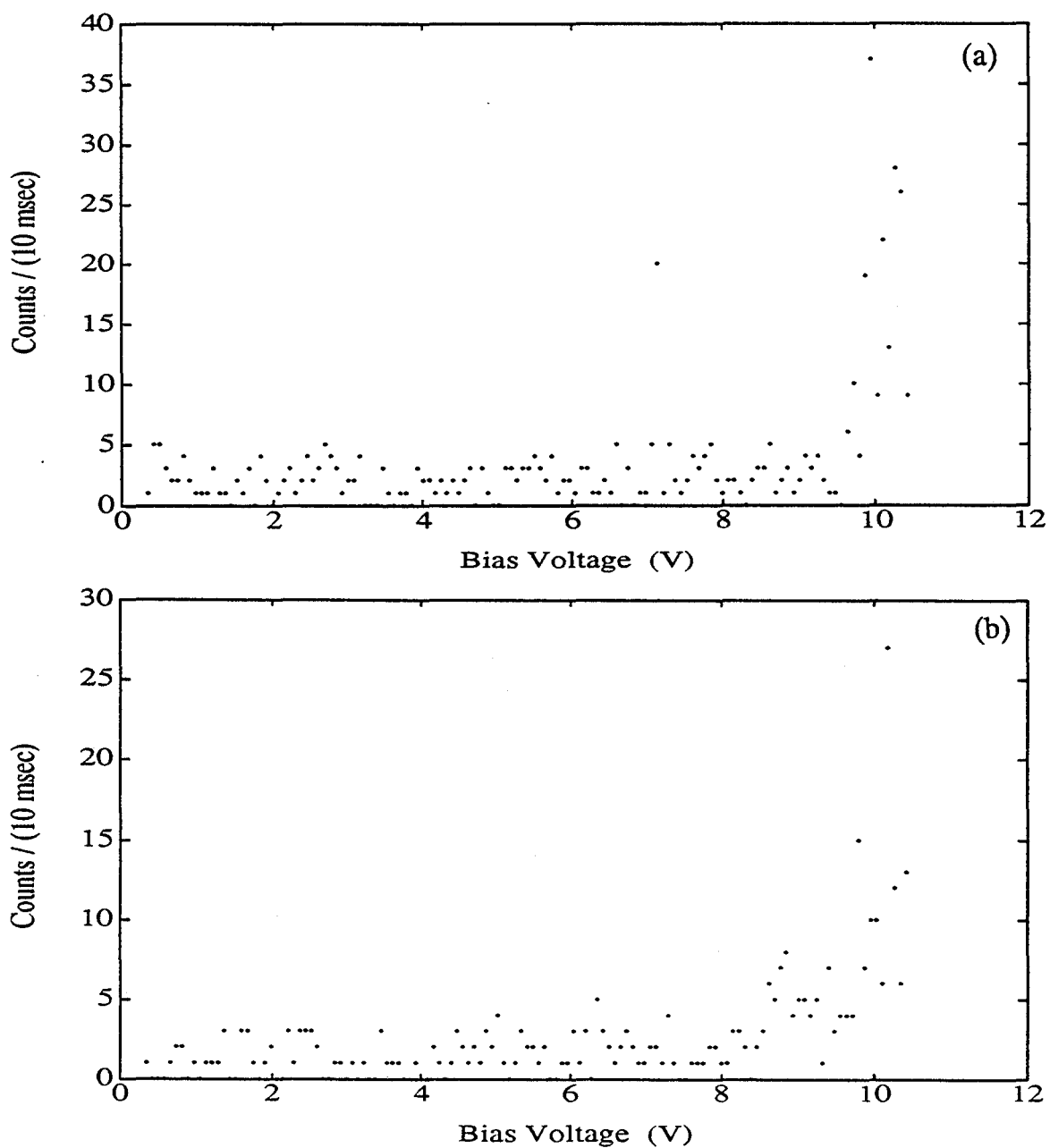
FIG. 22. The plot of the collector current versus the bias voltage. The bias voltage was swept from 0.293 Volts to 10.5 Volts. The data was taken at room temperature, 10^{-8} torr pressure, and with coordinates x = 100, and y = 65. (a) Upward bias voltage motion. (b) Downward bias voltage motion.

than 5 volts. During this measurement, the pressure inside the chamber was about 1 x 10^{-7} torr. We have performed similar measurements with a 60 nm-thick, annealed gold film. The results are essentially similar to the results obtained for 40 nm-thick film except that the collector currents are generally smaller. One typical curve obtained for the 60 nm-thick film is shown in Fig. 23. From the minimum value of the threshold voltage that can be extracted from the data shown in Figs. 17-23, we can assign an upper limit of 5.2 V, for the work function of Au.

In Figures 24-26 we show the time dependence of the collector current. The sample is the same 40 nm-film used to obtain the results that are shown in Figs. 17-19. In this measurement, we first turned off the feedback, then we increased the tunnel bias to about 11 V, and then we measured the collector current 128 times in 10 msec intervals. At the end, we changed the bias voltage back to the original value, and then we turned on the feedback again. The figures shown are successive measurements at the same spot of the sample. These data, together with the data of the previous experiment, show that the collector current, or the emission of ballistic electrons a) goes down very rapidly with time and b) has an unpredictable behavior. This behavior is not expected from a clean metal surface. The exact mechanism that shuts down the collector current is not clear to us. However, we looked into several possibilities. First, we looked into the sample heating
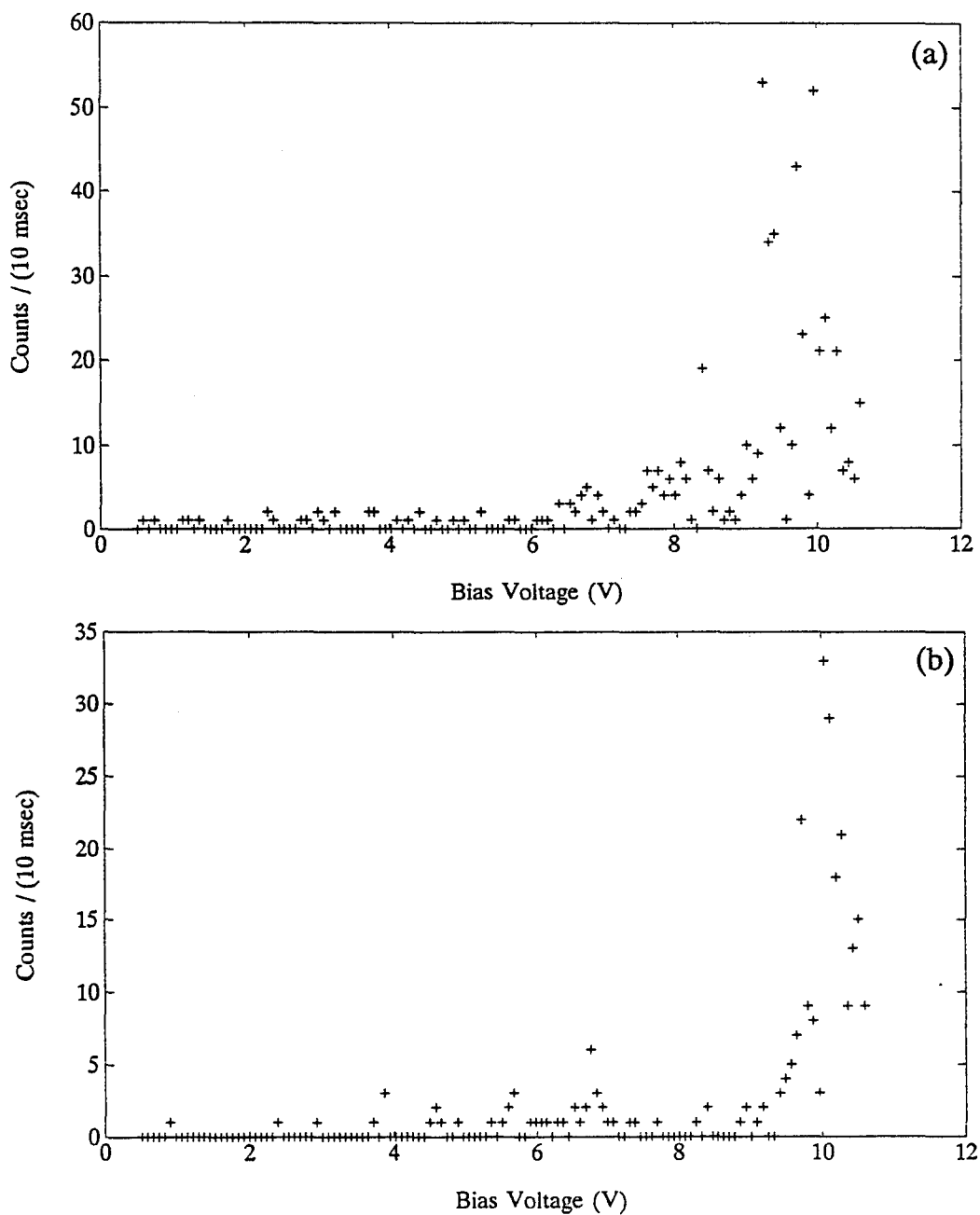
FIG. 23. The plot of the collector current versus, the bias voltage. The bias voltage was swept from 0.35 Volts to 10.5 Volts. The data was taken at room temperature, 10^{-8} torr pressure. (a) Upward bias voltage motion, (b) Downward bias voltage motion.

FIG. 24. The plot of the collector current versus time. The bias voltage was increased to 10 Volts and the collector current versus time was plotted. Each data point was taken in 10-msec time intervals and at coordinates x = 0, and y = 0.

FIG. 25. The plot of the collector current versus time. The bias voltage was increased to 10 Volts and the collector current versus time was plotted. Each data point was taken in 10-msec time intervals and at coordinates x = 0, and y = 0.
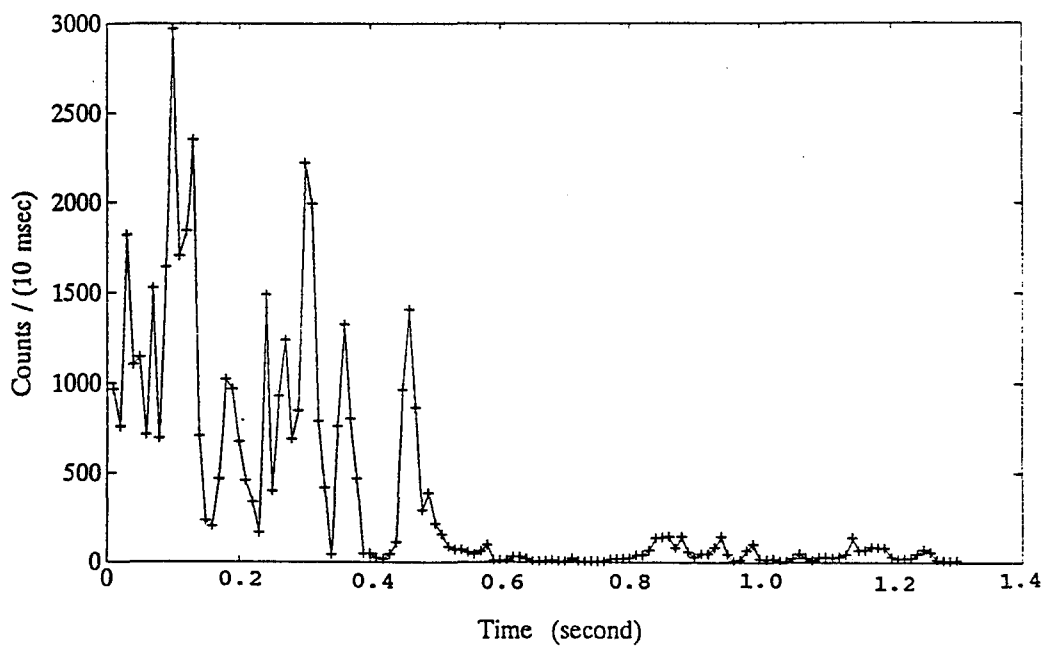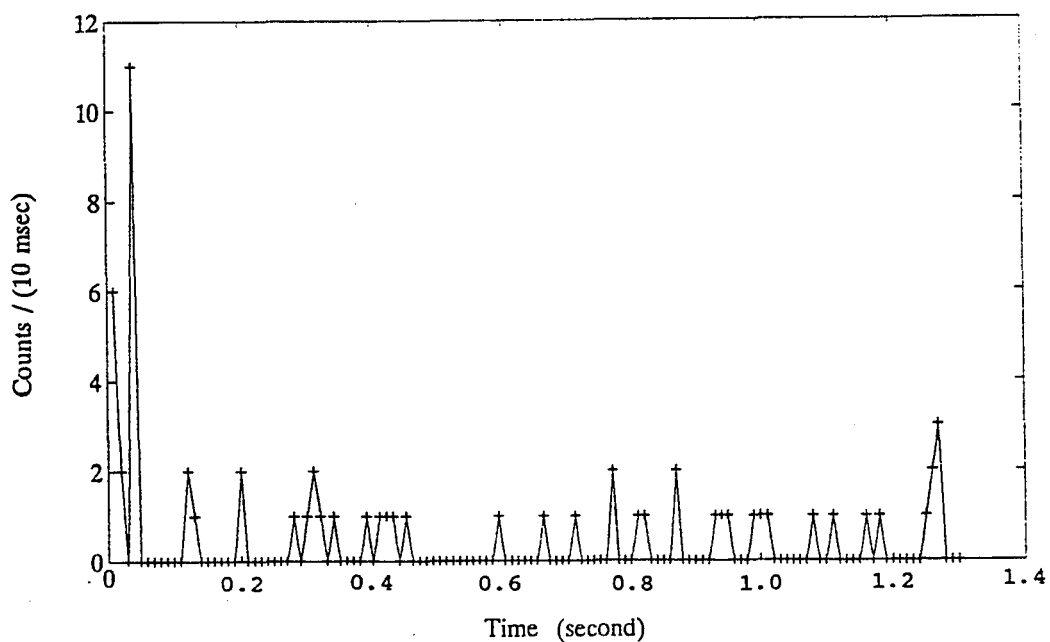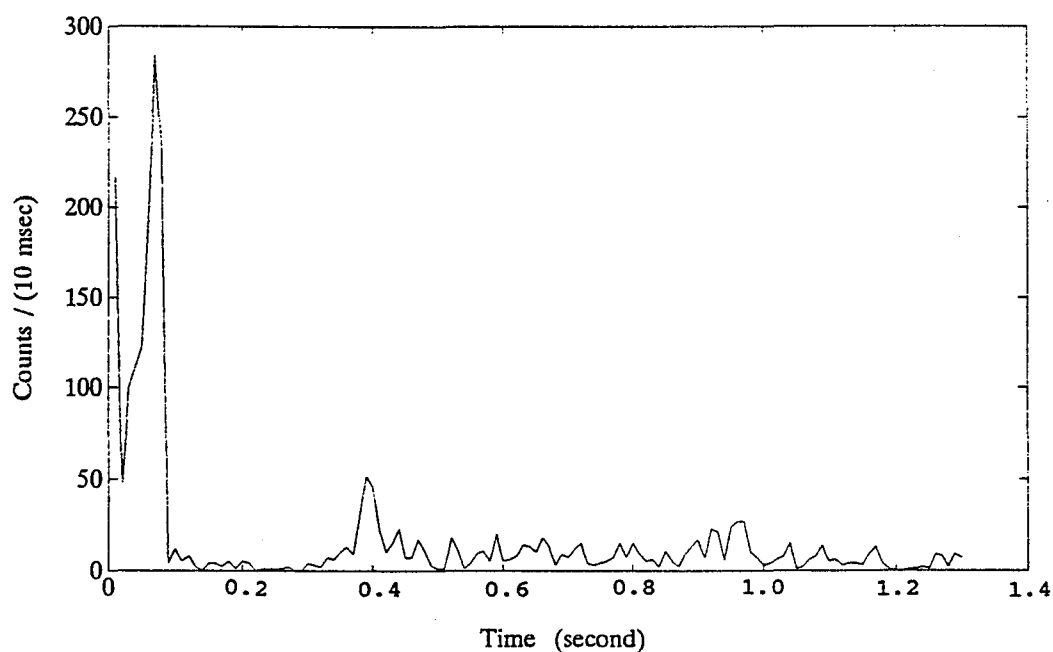
FIG. 26. The plot of the collector current versus time. The bias voltage was increased to 10 Volts and the collector current versus time was plotted. Each data point was taken in 10-msec time intervals and at coordinates x = 0, and y = 0.

behavior that we observed. We can model the heat generation by the tunnel current as a cylindrical source of heat, whose diameter is 1 nm (width of the current beam), and whose height is the same as the film thickness t, and which is located at the center of our film. If we take a tunnel current of 1 nA at a tunnel bias of 5 V, then the power generated can be taken as P = 5 x 10^{-9} W. If we assume that all the heat conducts out radially, we can solve the equation for the heat conductivity to obtain

$$T_i - T_o = (\frac{P}{2\pi k t}) \ln (\frac{r_o}{r_i}) \tag{5}$$

where T_i and T_o are the temperatures at radii r_i and r_o from the axis of the heat source, respectively. The thermal conductivity of the film is k. Assuming that at r_o = 1000 nm, the temperature is almost room temperature, t = 40 nm, and the thermal conductivity of Au is k = 380 W/m.K, then the temperature at the surface of the heat source is about 0.4 mK above room temperature. Even if one uses k = 0.026 W/m.K, the thermal conductivity of air, this temperature is no more than a few K above room temperature. Thus we can rule out any effects due to heating.

We can think of the decay of the collector current as arising from some sort of contaminants residing either on the surfaces or in the vacuum. With a bias voltage of about 5 V and a tunnel current of 1 nA, the tip-sample spacing may be somewhere between 1-2 nm.[38] Under the strong, non-uniform

electric fields present in the tip-sample region, contaminants may be attracted to the region between the tip and the sample. The motion of atoms under the force fields of the tip has been well-demonstrated. For example, Eigler et al. manage to arrange xenon atoms on a substrate by using an STM tip.[39] These contaminants may scatter the tunneling electrons changing their energy and momenta. This can cause the collector current to decay with time. The fact that the collector current decays in a time period of a few hundred milliseconds means that contamination needs a time of that order to gather. Some of the contaminations may undergo decomposition and polymerization due to the electrons bombarding them. Ehrichs et al. have fabricated nanometer scale patterns of such contaminations by applying -5 V pulses to an STM tip.[15] Thus we contend that contamination pile-up at the tunnel junction may be a possible mechanism for the decay of the collector current.

We can conjecture another possible mechanism for the decay of the collector current. In this mode, we imagine a presence of a contaminant layer in the back of the metal film. Some of the electrons that leave the base may get trapped in this contaminant layer forming a layer of negative charge. This charge layer can raise the effective barrier that an electron experiences. We can make a rough estimate of the effect of such a charge layer as follows. Assume a negative charge layer that is 1 nm away from the metal surface. This layer can be regarded as inducing a layer of positive charge on the surface of the

metal, effectively forming a dipole layer. If the energy necessary for an electron to cross this dipole layer is W, in the units of eV, using some formulae from electrostatics, we can write the surface charge density of the layer as 0.00885 x W in the units of C/m^2. Here, we have assumed the dielectric constant to be unity. This charge density in the units of electrons/nm^2 is 0.055 x W. Thus if W = 5, then we need 2.5 electron/nm^2. If the CEM is receiving 10^4 electron/s, and if we take that the electrons are exiting through an area 100 nm^2, 100 electrons pass an area 1 nm^2 every second. Thus if electron trapping occurs at an efficiency of 0.6%, then an effective barrier of 5 eV can be formed in 0.5 s.

At present, we do not have enough information to confirm whether any of the above mechanisms is correct. However, we can say that if our metal surface is absolutely clean, the collector current should not decay. At present, our ultimate vacuum is limited to 1 x 10^{-8} torr. This limit is due to out-gassing of the circuit components of the CEM. At this pressure, a monolayer can be formed in less than 3 minutes. Therefore, we cannot expect to perform experiments at ultra clean conditions. However, as the collector current decays in a time interval of a few tenths of a second, we still can carry out experiments using fast measurements (about 10 msec).

We also tried to obtain images through the use of the collector current by X-Y scanning the tip over the sample at the constant tunnel current feedback mode. We set the tunnel bias

at a value that yields a suitable collector current. We mapped
the collector current as the tip performed the X-Y scan. Figure
27 shows such a map obtained on a 40 nm-thick, unannealed
sample. The scan size is 200 nm x 200 nm and the tunnel bias
was 11 V. One can see areas of very high collector current.
This demonstrates the possibility of using the collector current
for imaging purposes. However, except for this particular
image, we have not been able to produce collector current images
that show clear features. We believe that the aforementioned
effects due to contaminants and/or charging may have
overshadowed the effects due to sample irregularities.

Even though the collector current dies down within a few
tenths of a second when the tip is stationary over the sample,
while the tip is scanning, we can have a persistent, although
fluctuating, collector current. This is understandable since
while scanning, the tip may not stay at one point long enough
for the process that turns off the collector current to be
complete. We took advantage of this fact to obtain a crude
value for the work function of the sample, that is an average
over the scanned area. To do this, we averaged the collector
current over the scanned area, which was 375 nm x 375 nm, for
several tunnel biases. The sample was a 60 nm-thick annealed Au
film. The results are plotted in Fig. 28. The count rate is
small because of the averaging over high and low values of
collector current that occurred during the scan. It can be seen
that the collector current starts to rise at a bias voltage
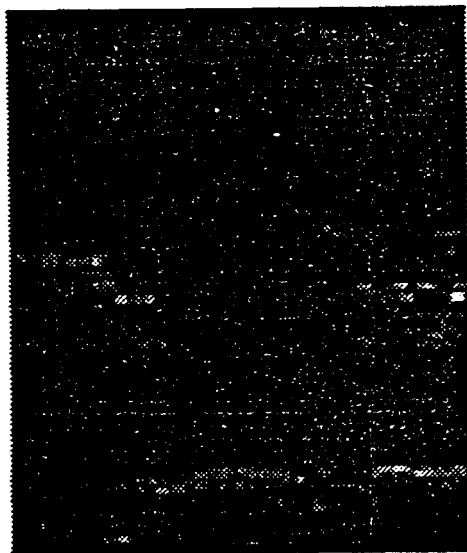
(a)
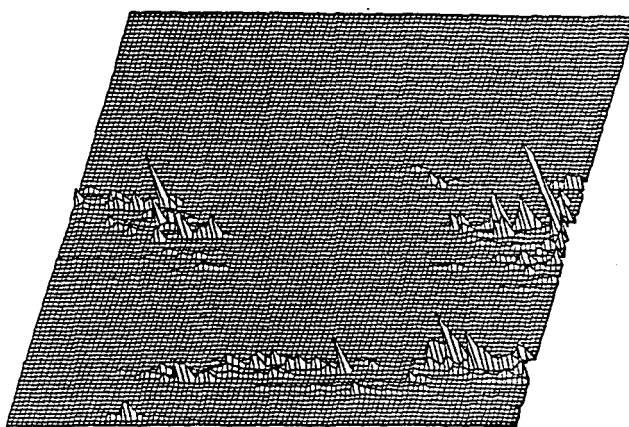
(b)

FIG. 27. A map of the collector current obtained on a 40 nm-thick, unannealed sample. The scan size is 200 nm x 200 nm and the bias voltage is 11 V.
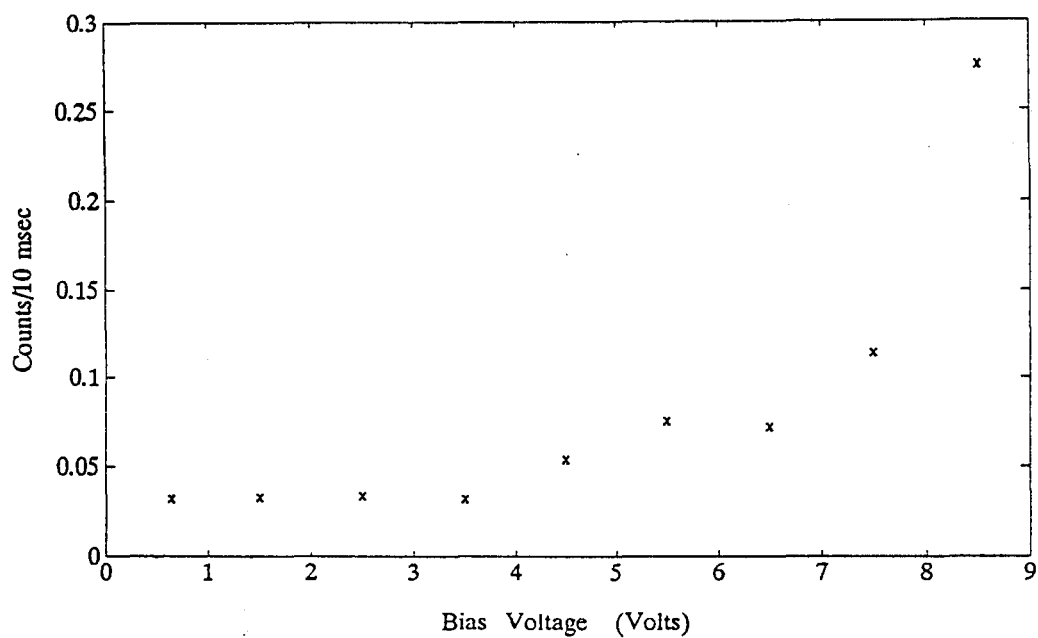
(a) Gray scale representation, (b) Perspective view

FIG. 28. Collector current versus bias voltage. The collector current was averaged over the scanned area. The scan size is 375 x 375 nm.

somewhere around between 3.5 V and 4.5 V. This result again demonstrates the ability of our set-up to study the properties of the metal surface.

CHAPTER V

CONCLUSIONS

In conclusion we have demonstrated the possibility of using the ballistic electron emission phenomenon to study the metal-vacuum interface. In order to achieve this goal, we have built a novel ballistic electron emission microscope (BEEM) inside an ultra high vacuum chamber. This BEEM uses a channel electron multiplier to detect the collector current. We used our instrument to get an upper limit to the work function of Au. This value falls within the literature values for the work function of Au. Our present vacuum conditions and sample cleanliness do not allow us to make detailed measurements of the work function variations over sample surfaces. However, we believe that our work is the first step towards that goal. Further, we have shown the feasibility of imaging the variation of sample surface properties through the use of BEEM.

Also in our investigation, we have established a procedure to prepare thin, free-standing gold films that are free of holes and consists of grains that are much larger than the thickness

of the sample. We have shown that these samples are strong enough to be imaged by a scanning tunneling microscope in air and in high vacuum. We believe that our work will pave the way to studies of surface properties with very high spatial resolution.

References

1. G.Binnig, H. Rohrer, Ch. Gerber, and E. Weibel, Phys. Rev. Lett. **49**, 57 (1982).

2. Y. Kuk and P.J. Silverman, Rev. Sci. Instrum. **60**, 165 (1989)

3. G. Binnig, H. Rohrer, Ch. Gerber and E. Weibel, Phys. Rev. Lett. **50**, 120 (1983).

4. R.J. Hamers, R.M. Tromp and J.E. Weibel, Phys. Rev. lett. **56**, 1972 (1986).

5. E.L. Wolf, Principles of Electron Tunneling Spectroscopy (Oxford University Press, New York, 1985).

6. J. A. Stroscio, R. Feenstra, A. P. Fein, Phys. Rev. Lett. **57**, 2579 (1986)

7. H.G. Le duc, W.J. Kaiser and J.A. Stern, Appl. Phys. Lett. **50**, 1921 (1987).

8. K. W. Ng., A. L. de Lozanne, J. M. Tarascon and L.H. Greene, Surface Science B **35**, 7220 (1987).

9. Z.Y. Rong, L. Cohen and E.L. Wolf, Phys. Lett. A **146**, 281 (1990).

10. Ph. Avouris, In-Whan Lyo, F. Bozso, J. Vac. Sci. Technol. B **9**, 424 (1991).

11. A. J. Bard, F. R. F. Fan, J. Kwak, and O. Lev, Anal. Chem. **61**, 132 (1989).

12. S. Morita, I. Otsuka, T. Okada, H. Yokoyama, T. Iwasaki, and N. Mikoshiba, Jpn. J. Appl. Phys. **26**, L1853 (1987).

13. A. M. Baro, R. Miranda, J. Alanman, N. Garcia, G. Binnig, H. Rohrer, Ch. Gerber and J. L. Carrascosa, Nature **315**, 253 (1985).

14. A. M. Baro, R. Miranda, J.L. Carrascosa, IBM J. Res. Develop. Vol. **30**, 340 (1986)

15. E.E. Ehrichs, S. Yoon, and A. L. de Lozanne, Appl. Phys. Lett. **53**, 2287 (1988).

16. W.J. Kaiser, L.D. Bell, Phys. Rev. Lett. **60**, 1406 (1988).

17. L.V. Azároff, J.J. Brophy, Electronic Processes in Materials, (McGraw-Hill, Inc. 1963).

18. C. Kittel, Introduction to Solid State Physics, 5th edition, (John Wiley and Sons, 1976)

19. M. H. Hecht, L. D. Bell, W. J. Kaiser, and F. J. Grunthaner, Appl. Phys. Lett. **55**, 780 (1989).

20. L.D. Bell, W.J. Kaiser, Phys. Rev. Lett. **61**, 2368 (1988)

21. M.H. Hecht, L.D. Bell, and W.J. Kaiser, Phys. Rev. B **42**, 7663 (1990)

22. L.D. Bell, M.H. Hecht, and W.J. Kaiser, Phys. Rev. Lett. **64**, 2679 (1990)

23. N. W. Ashcroft, N. D. Mermin, Solid State Physics, (Saunders College, PA, 1976).

24. Handbook of Chemistry and Physics, 72nd edition, edited by D. R. Lide, (CRC Press, Inc., Boca Raton, 1991) p. 12-97.

25. P. West, J. Kramar, D. V. Baxter, R. J. Cave and J. D. Baldeschwieler, IBM J. Res. Develop. **30**, 484 (1986).

26. J. K. Gimzewski and R. Moller, Phys. Rev. B **36**, 1284 (1987).

27. G. Binnig, H. Rohrer, Ch. Gerber, and E. Weibel, Appl. Phys. Lett. **40**, 178 (1982).

28. F. Real, Ph.D. Thesis, Polytechnic University (1993).

29. H. Jonathan Mamin, Eric Ganz, David W. Abraham, Ruth Ellen Thomson, and John Clarke, Phys. Rev. B **34**, 9015 (1986).

30. S. M. Lindsay, Y. Li, J. Pan, T. Thundat, L. A. Nagahara, P. Oden, J. A. DeRose, U. Knipping, and J. W. White, J. Vac. Sci. Technol. B **9**, 1096 (1991).

31. G. Binnig and D. P. Smith, Rev. Sci. Instrum. **57**, 1688 (1986).

32. Modern Piezoelectric Ceramics, PD-9247, a publication from Vernitron Piezoelectric Division, OH., p. 2.

33. G. A. Somorjai, The Structure and Chemistry of Solid Surface (John Wiley, New York, 1969).

34. L. D. Bell, W. J. Kaiser, M. H. Hecht, Scanning Tunneling Microscopy, (Editors; J. A. Stroscio, W. J. Kaiser)

35. M. Prutton, Surface Physics, (Oxford University Press, 1983), p. 83

36. C. D. Hodgman, R. C. Weast, R. S. Shankland, S. M. Selby, Handbook of Chemistry and Physics, forty - fourth edition, p.2238 - 2239, (The Chemical Rubber Publishing Co., Ohio, 1962)

37. R. C. Jacklevic, L. Elie, W. Shen, J. T. Chen, J. Vac. Sci. Technol. A **6**, 448 (1988).

38. R. Young, J. Ward, and F. Scire, Rev. Sci. Instrum. **43**, 999 (1972)

39. D. M. Eigler, P. S. Weiss, E. K. Schweizer, N. D. Lang, Phys. Rev. Lett. **66**, 1189 (1991).